Empirical density-dependent effective interaction for nucleon-nucleus scattering at 500 MeV

B. S. Flanders
Department of Physics, American University, Washington, D.C. 20016

J. J. Kelly and H. Seifert
Department of Physics and Astronomy, University of Maryland, College Park, Maryland 20742

D. Lopiano,[a] B. Aas,[b] A. Azizi,[c] G. Igo, G. Weston,[d] C. Whitten, and A. Wong[e]
Department of Physics, University of California at Los Angeles, Los Angeles, California 90024

M. V. Hynes and J. McClelland
Los Alamos National Laboratory, Los Alamos, New Mexico 87545

W. Bertozzi, J. M. Finn,[f] C. E. Hyde-Wright,[g] R. W. Lourie,[h] B. E. Norum,[h] and P. Ulmer[i]
Department of Physics and Laboratory for Nuclear Science, Massachusetts Institute of Technology, Cambridge, Massachusetts 02139

B. L. Berman
Department of Physics, George Washington University, Washington, D.C. 20052
(Received 21 December 1990)

We report new cross-section and analyzing-power data for the excitation by 498-MeV protons of all narrow normal-parity states of ^{16}O below 12.1-MeV excitation. In addition, spin-rotation measurements for elastic scattering and depolarization measurements for the 1_1^-, 2_1^+, and 3_1^- states of ^{16}O have been performed. These data are used in conjunction with existing data for ^{40}Ca to study medium corrections to the effective interaction for nucleon-nucleus scattering at 500 MeV. Systematic differences between the data and nonrelativistic impulse approximation calculations based upon either the free t matrix or a recent density-dependent effective interaction are interpreted within the framework of the local-density approximation. An empirical effective interaction has been constructed which parametrizes the density dependence of the medium modifications in a simple form amenable to phenomenological analysis of data. The parameters of the interaction are adjusted by fitting to data from many transitions simultaneously, including inelastic transitions sensitive to both the surface and the interior of the nucleus. We find that the empirical effective interaction provides a good description of both the fitted inelastic-scattering observables and elastic-scattering observables not included in the fit. Furthermore, we find that the empirical effective interaction fitted to inelastic-scattering data for ^{16}O provides an excellent description of both elastic- and inelastic-scattering data for ^{40}Ca at 500 MeV. The most significant difference between the empirical interaction and the theoretical interaction is that absorption is enhanced at higher density, contrary to expectations based upon Pauli blocking. We find also that the empirical interaction has a stronger repulsive core than expected in nonrelativistic models of the effective interaction. Nevertheless, the optical potentials are very similar to the Schrödinger-equivalent potentials from a relativistic impulse approximation model, showing that the empirical density dependence is comparable to the equivalent density dependence due to elimination of lower components from this relativistic model of the nucleon-nucleus interaction. These results are also compared with global optical potentials from Dirac phenomenology, which suggest even stronger repulsion in the real central interaction.

I. INTRODUCTION

The interpretation of nucleon-nucleus scattering at intermediate energies has relied largely on phenomenological representations of the coupling between the projectile and target nucleons. One approach that has been used widely is the introduction of an effective interaction.[1] In the nonrelativistic impulse approximation (NRIA), this interaction is taken to be the free N-N t matrix.[2] Although the NRIA provides a good basis for the investigation of many aspects of nucleon-nucleus interactions, it has been shown to give poor predictions of scattering observables in many cases.[3] Improvements to the predictions in the NRIA for 500-MeV incident protons have been made by the inclusion of modifications due to the nuclear medium[4] and/or relativistic effects.[5]

Beyond the IA, the interaction between a projectile nucleon and a target nucleon has been shown to depend strongly on the nuclear density in the region of the interaction.[6] Several groups have constructed density-dependent effective interactions for infinite nuclear matter[7–9] following the G-matrix approach of Hüfner and Mahaux.[10] These interactions are generally applied to calculations of scattering observables using the local-density approximation (LDA), which assumes that the effective interaction in the nuclear medium can be approximated by the interaction calculated in infinite nuclear matter at the same local density. The accuracy of this approximation, the LDA, has not been established. Since nuclear orbitals pervade the entire nucleus, it is reasonable to expect that the interaction will have knowledge of and sensitivity to a spectrum of nuclear densities.

G matrices from several nuclear matter calculations for incident energies below about 300 MeV have been available for several years and calculations of inelastic scattering with these interactions show considerable improvement with respect to calculations in the NRIA.[11] Recently, Ray has produced an effective interaction[4] based upon the Watson optical model[12] and a meson-exchange potential.[13] In addition to the Pauli blocking and nuclear binding effects included in earlier calculations, this model includes NN inelasticity through pion production and coupling to isobars. Hence this theoretical interaction is applicable to higher energies (300–800 MeV). Ray showed that predictions of elastic-scattering observables with this interaction were improved relative to the NRIA. Calculations of inelastic scattering at 500 MeV with this interaction show improvements with respect to calculations with a free interaction also, but the improvements are modest and modifications are required to produce a good description of the data.

In the energy regime 100–300 MeV, the differences between the various nuclear matter interactions are significant; the dependencies on density are qualitatively similar, but the predictions of scattering observables are significantly different.[11] Although nucleon inelastic scattering for incident energies between about 200 and 500 MeV has been shown to possess good intrinsic radial sensitivity,[14] permitting the extraction of neutron transition densities even in the nuclear interior, the accuracy of these determinations is limited by the residual errors in the effective interaction.

Therefore, we have developed a parametrized model for the effective interaction, guided by nuclear matter theory, that can be fitted to inelastic-scattering data for many transitions simultaneously.[15–17] To minimize uncertainties due to nuclear structure, we restrict ourselves to normal-parity isoscalar transitions for which accurate transition charge densities are available from electron-scattering measurements and for which the transverse form factors are negligible. For self-conjugate targets, charge symmetry ensures that neutron and proton transition densities are very nearly equal so that the nuclear structure relevant to these excitations is determined unambiguously. If the concept of a local nuclear matter density is valid, a single set of parameters should describe all direct, isoscalar normal-parity transitions simultaneously, independent of the target nucleus. By using a data set that includes states with transition densities of both interior or surface character, we obtain sensitivity to the density dependence of the effective interaction. By comparing interactions fitted to data for several nuclei independently or by fitting data for several nuclei simultaneously, we test the applicability of the local-density approximation.

The results of this approach have been reported[15–17] for 135-, 180-, and 318-MeV incident protons and are underway for incident proton energies of 100 and 200 MeV.[18] Below 300 MeV we find that the energy dependence of the empirical interaction is smooth and is similar to the predictions of nuclear matter theory. At 318 MeV, on the other hand, we find that absorption at high density, which is expected to be suppressed by Pauli blocking, appears to be slightly enhanced instead. We also find that the strength of the density-dependent repulsive core is considerably stronger than predicted by non-relativistic models of the effective interaction.

An alternative description of nucleon-nucleus scattering is provided by the relativistic impulse approximation (RIA) based upon the Dirac equation.[19] Perhaps the most appealing characteristic of this model is its ability to consistently describe spin-dependent observables, such as the analyzing power (A_y) and spin-rotation function (SRF).[20–23] In fact, much of the initial impetus for development of RIA models was the successful description of A_y and SRF for $p+{}^{40}$Ca at 500 MeV by Dirac phenomenology,[20] quantities which are poorly described by the NRIA based upon the free interaction. Subsequently, it has been found that both RIA and NRIA give similar results above 650 MeV,[5] and that both models require substantial Pauli blocking corrections below 300 MeV.[22] Hence the most dramatic divergence between these approaches remains in the vicinity of 500 MeV.[4]

Given comparable descriptions of free NN scattering, the primary difference between the NRIA and RIA models of elastic scattering is related to behavior of virtual $N\bar{N}$ pairs in the medium.[23] Potentials for use in the Schrödinger equation which give the same results as the RIA can be derived by elimination of lower components of the Dirac spinors.[20,21] Ottenstein, Wallace, and Tjon[5] have performed a systematic analysis of elastic scattering in the RIA using a meson-exchange model[24] designated IA2 and find that the $N\bar{N}$ contribution to the Schrödinger-equivalent potentials can be described as a repulsive density-dependent contribution to the effective interaction. We found that at 318 MeV these IA2 potentials are in fact quite similar to the optical potentials that emerge from the empirical effective interaction fitted to inelastic-scattering data using our nonrelativistic model.[17] Therefore, it appears that the strong repulsive core in the empirical interaction may have a relativistic origin. However, the apparent absence of Pauli blocking is not explained and may require a new absorptive mechanism, perhaps related to pion production.

In this work we extend to 500 MeV the investigation of medium modifications to the effective interaction. We use inelastic scattering observables from 500-MeV

$\vec{p}+{}^{16}\mathrm{O},{}^{40}\mathrm{Ca}$ to deduce the coefficients in an empirical parametrization of the density dependence of the effective interaction. In addition to cross-section and analyzing-power data used for lower energies, depolarization and spin-rotation data are available for several states and were fitted also. We find the empirical interaction describes the data over a wide range of momentum transfer for all ten transitions that we consider. In addition, the interaction fitted to inelastic transitions provides a good description of elastic-scattering observables for both ^{16}O and ^{40}Ca. We find that substantial modifications to the free interaction are required and that there is a strong density-dependent enhancement of both the real and imaginary parts of the isoscalar spin-dependent central component of the interaction. In fact, the anomalous enhancement of absorption at high density is even stronger at 500 than at 318 MeV. Nevertheless, the optical potentials continue to agree with Schrödinger-equivalent IA2 potentials.

The experimental procedure and data analysis are presented in Sec. II. Our model and parametrization are described briefly in Sec. III. We present our results with a comparison of the predictions based on the NRIA, the Ray interaction, and our empirical interaction in Sec. IV. Section IV also includes a discussion of possible ambiguities in the fitted interaction and several alternative models of the density dependence. Section V compares our results with those of other approaches, including the relativistic impulse approximation and Dirac phenomenology. Comparisons between nonrelativistic and relativistic models, such as the IA2 model, are made through Schrödinger-equivalent optical potentials. We summarize our conclusions in Sec. VI.

II. EXPERIMENT

The experiment was performed at LAMPF using the high-resolution spectrometer (HRS) and its focal-plane polarimeter (FPP). Detailed descriptions of these apparatuses may be found in Refs. 25 and 26. Protons beams with 497.5 MeV kinetic energy impinged upon BeO foils with thicknesses ranging between about 24 and 200 mg/cm^2. In addition, two Be foils (26.8 and 47.3 mg/cm^2) were used to collect data upon the beryllium continuum below the oxygen states of interest. Ionization chambers were used to monitor the beam intensity and were normalized by comparing elastic pp measurements made using thin CH_2 targets to calculations based upon the Arndt phase shifts.[27]

Measurements were made with beams polarized normal to the scattering plane (N type), along the beam direction (L type), and in-plane but orthogonal to the beam (S type). The beam polarization was monitored using the line-C polarimeter, which measures components orthogonal to the beam, and the quench ratio.[28] Average polarizations of about 80% were obtained. Approximately 100 h of running time were required with average beam currents of 1–2 nA in each of the three orientations. Data were collected for laboratory angles between about 6° and 33° in steps of about 2°. Spectra for N-type beam were made for the central 2° of the HRS angular acceptance for each spectrometer setting. For L- and S-type beams, the 2° bins were subdivided into three equal parts so that finer angular resolution in the depolarization observables could be obtained for the strongest states.

The spectra were analyzed using the line-shape fitting program ALLFIT (Ref. 29) and methods described in Ref. 11. The ^{9}Be continuum was described using the positions and widths deduced by Dixit *et al.*[30] and amplitudes determined from spectra obtained with a ^{9}Be target, when available. Narrow peaks of ^{16}O were described by the standard hyper-Gaussian line shape. Peaks with intrinsic widths[31] larger than 20 keV were described by Lorentzian shapes convoluted with a resolution function based upon the narrow peaks. Further details of this analysis may be found in Ref. 32.

The polarization at the focal plane was determined using the weighted sums method described in Refs. 33 and 34. The depolarization parameters were then deduced by correcting for precession of the spin through the HRS dipoles and adjusting for the incident polarization. Consistency checks are provided by the symmetry relations

$$P = A_y \ , \tag{1a}$$

$$D_{LS} = -D_{SL} \ , \tag{1b}$$

$$D_{LL} = D_{SS} \ , \tag{1c}$$

$$D_{NN} = 1 \ , \tag{1d}$$

where D_{if} describes the transfer of initial polarization $\hat{i}$ to final polarization $\hat{f}$, and where L and S always refer to the coordinate systems for which L is along the momentum of the particle. The first three relations must always be satisfied for elastic scattering, and the last is also required for elastic scattering from spinless targets. For the most part these relationships are satisfied by our data within their estimated uncertainties.

Since there are only two independent polarization transfer coefficients for elastic scattering, it is customary to report the analyzing power A_y and a spin-rotation function (SRF) defined as the depolarization coefficient D_{zx}, where the (x,y,z) coordinate system coincides with the $(S,N,L)_i$ coordinate system in the laboratory. The depolarization parameter D_{zx} is often designated Q and is related to the angle β through which the projection of the polarization upon the scattering plane is rotated by

$$\sin\beta = \frac{Q}{(1-P^2)^{1/2}} \ . \tag{2}$$

Depolarization parameters could be obtained for elastic scattering and for the three strong low-lying inelastic transitions, namely, the 3_1^- (6.130 MeV), 2_1^+ (6.917 MeV), and 1_1^- (7.117 MeV). In addition, cross-section and analyzing-power data were obtained for the 0_3^+ (12.053 MeV), 2_2^+ (9.847 MeV), 2_3^+ (11.52 MeV), 2_1^- (8.872 MeV), and 4_1^+ (10.353 MeV) states. Finally, data were obtained for the unresolved $(3_1^+,4_2^+)$ doublet at 11.09 MeV. Complete data tables are on deposit with the Physics Auxiliary Publication Service (PAPS).[35]

III. EMPIRICAL EFFECTIVE INTERACTION

In this section we describe briefly the linear expansion model used for our analysis. Complete descriptions of the linear expansion technique may be found in Refs. 14, 15, and 36, the reaction model in Ref. 37, and the approximations we make in Ref. 11.

A. Reaction model

Our application is based upon the local nonrelativistic distorted-wave approximation presented in Ref. 11. This work is limited to isoscalar normal-parity transitions driven by the proton and neutron matter densities. For ^{16}O we use the transition densities fitted to longitudinal form factors measured by Buti *et al.*[38] For ^{40}Ca we use the densities fitted by Miskimen[39] to the unpublished electron-scattering data of Ref. 40. Since the transverse form factors for all transitions considered are very small, we assume that all spin and current densities, including those not sampled by electron scattering, are negligible. Then transition densities from the electron-scattering measurements were corrected for the nucleon form factor and used to specify the nuclear structure (densities) with little uncertainty, under the assumption of charge symmetry.

With these restrictions the effective interaction (t) reduces to central (C) and spin-orbit (LS) components:

$$t(q)=t^{C}(q)+it^{LS}(q)\boldsymbol{\sigma}\cdot\hat{\mathbf{n}} , \tag{3}$$

where $\boldsymbol{\sigma}$ describes the projectile spin and $\hat{\mathbf{n}}$ is the unit vector normal to the scattering plane. It is convenient to introduce the quantity τ^{LS}, where

$$t^{LS}=-\frac{qQ}{2}\tau^{LS}=-(k^2\sin\theta)\tau^{LS} , \tag{4}$$

and $\mathbf{q}=\mathbf{k}_i-\mathbf{k}_f$ and $\mathbf{Q}=\mathbf{k}_i+\mathbf{k}_f$ are the direct and exchange momentum transfers, respectively. [The Q in Eq. (4) is not the same as the Q in Eq. (2).] Exchange contributions are evaluated using a local approximation.[11]

For normal-parity isoscalar transitions, the scattering potential can be expressed as

$$U(\mathbf{r})=U^{Z}(\mathbf{r})+U^{c}(\mathbf{r})+\boldsymbol{\nabla}F^{LS}(\mathbf{r})\otimes\frac{1}{i}\boldsymbol{\nabla}\cdot\boldsymbol{\sigma} , \tag{5}$$

where U^Z is the potential obtained from the folding of the appropriate transition density with the Coulomb interaction. For any transition J, the spin-independent central (U^C) and spin-orbit (F^{LS}) terms can be expressed in the $t\rho$ form as

$$U_J^{C}(r)=\eta\frac{2}{\pi}\int dq\, q^2 j_J(qr)t^{C}(q,k_F)\tilde{\rho}_J(q) , \tag{6a}$$

$$F_J^{LS}(r)=\eta\frac{2}{\pi}\int dq\, q^2 j_J(qr)\tau^{LS}(q,k_F)\tilde{\rho}_J(q) , \tag{6b}$$

where $\tilde{\rho}_J(q)$ is the matter transition density in momentum space. Here the factor η is the Jacobian for transforming from the nucleon-nucleon frame to the nucleon-nucleus frame and is near unity.[1,2] These forms include density dependence by evaluating the interactions t^C and τ^{LS} at the nuclear density (Fermi momentum k_F) corresponding to the position of the projectile. For self-conjugate targets we assume that the local matter density is proportional to the appropriate ground-state charge density, corrected for the proton finite size, determined from the electron-scattering measurements compiled in Ref. 41. The choice of evaluating the interactions at the nuclear density corresponding to the position of the projectile, the position of the target nucleon, or the midpoint between the projectile and target nucleon has little effect on the calculations of the scattering observables.[11]

Similarly, the optical potential for elastic scattering has the form

$$U(r)=U^{Z}(r)+U^{C}(r)+U^{LS}(r)(\mathbf{L}\cdot\boldsymbol{\sigma}) , \tag{7}$$

where the spin-orbit component is related to the scattering potential by

$$U^{LS}(r)=\frac{1}{r}\frac{\partial F^{LS}}{\partial r} . \tag{8}$$

The same effective interaction is used for both the optical and inelastic-scattering potentials, except that the density dependence of the interaction is enhanced for inelastic scattering by a rearrangement factor[42,43]

$$t_{\text{inel}}(\rho)=\left[1+\rho\frac{\partial}{\partial\rho}\right]t_{\text{elas}}(\rho) \tag{9}$$

that effectively doubles the density dependence. This relationship, derived by Cheon, Takayanagi, and Yazaki,[42] has been found to be vital to a consistent description of both elastic and inelastic scattering based upon a common density-dependent interaction for the entire energy range 100–500 MeV.[15–17]

B. Effective interactions

The effective interaction used in most nonrelativistic calculations is based upon the nucleon-nucleon t matrix[2] or, for energies below 300 MeV, a G matrix that incorporates medium modifications to that interaction due to the presence of infinite nuclear matter.[7–9] For energies above 300 MeV, Ray has incorporated several effects due to the nuclear medium into a theoretical interaction for use in scattering calculations.[4] However, systematic discrepancies exist between the inelastic-scattering data and calculations performed with the Ray interaction. These discrepancies necessitate that phenomenological adjustments be applied to the interaction before it can be used to probe neutron transition densities.

An empirical density dependence for each component (t_i) of the effective interaction may be parametrized with the form[15]

$$t_i(q,\kappa_F)=(S-d\kappa_F^{\alpha})t_i^{f}(q,0)+\kappa_F^{\gamma}\sum_n b_n[1+(q/\mu_n)^2]^{-\beta} , \tag{10}$$

where $\kappa_F=k_F/1.33$ is the Fermi momentum (density) relative to saturation and where t^f represents the free nucleon-nucleon interaction (at zero density). The flexibility of this form allows us to describe accurately each term of all available G-matrix calculations and the Ray

interaction. These theoretical interactions are used to guide fits to data by restricting the number of free parameters to a manageable number while providing an initial estimate of their values. We choose the β exponents to be 1 for central components and 2 for spin-orbit components, which result from the appropriate Fourier transforms of the "Yukawa" terms in the t-matrix expansion. The ranges μ_n and exponents α and γ are chosen to optimize the description of the best available theoretical interaction with the smallest number of strength parameters b_n. For this work we use the t matrix fitted by Franey and Love[2] to phase-shift data for 515-MeV nucleons to represent the free interaction, $t_i^f(q,0)$.

For incident energies below about 300 MeV, we find that the interaction constructed by the Hamburg group using the Paris potential[8] (labeled PH) provides the best available theoretical description of elastic-scattering and normal-parity excitations. Above 300 MeV the theoretical interaction constructed by Ray uses a meson-exchange model to compute the density-dependent changes in the effective interaction and then applies these changes to an empirical t matrix based upon nucleon-nucleon phase shifts. Hence, by including inelasticity in the nucleon-nucleon interaction, this method extends the effective interaction to energies above the pion threshold. Whereas the effect of Pauli blocking is found to decrease rapidly as the energy increases, dispersive effects produce substantial changes in the real central interaction even at 800 MeV. In addition, coupling to delta isobars is included, but is found to be relatively unimportant.

A good representation of both the Ray interaction and G-matrix interactions for $E \leq 318$ MeV can be found with the reduced parametrization[15–17]

$$\mathrm{Re}t^C(q,\kappa_F)=S_1\mathrm{Re}t^C(q,0)+b_1\kappa_F^3\left[1+\left[\frac{q}{\mu_1}\right]^2\right]^{-1}, \tag{11a}$$

$$\mathrm{Im}t^C(q,\kappa_F)=S_2\mathrm{Im}t^C(q,0)-d\kappa_F^2\mathrm{Im}t^C(q,0)\ , \tag{11b}$$

$$\mathrm{Re}\tau^{LS}(q,\kappa_F)=S_3\mathrm{Re}\tau^{LS}(q,0)+b_3\kappa_F^3\left[1+\left[\frac{q}{\mu_3}\right]^2\right]^{-2}, \tag{11c}$$

$$\mathrm{Im}\tau^{LS}(q,\kappa_F)=S_4\mathrm{Im}\tau^{LS}(q,0)+b_4\kappa_F^3\left[1+\left[\frac{q}{\mu_4}\right]^2\right]^{-2}, \tag{11d}$$

with $\mu_1=2.0$ fm^{-1}, $\mu_3=6.0$ fm^{-1}, and $\mu_4=1.0$ fm^{-1}. [The f superscripts have been omitted from Eq. (11) to reduce clutter.] We note that the $\mathrm{Im}\tau^{LS}$ contribution is too small to permit variation of its density dependence so that we hold S_4 to 1.0 and b_4 to -1.92, the values obtained from fitting this model to the Ray interaction. Therefore, we analyze our data using fix free parameters (S_1,b_1,S_2,d,S_3,b_3).

The isoscalar spin-independent central and isoscalar spin-orbit components of Ray's theoretical interaction for 500-MeV protons is shown in Fig. 1 for $k_F=0.0$, 0.7, and 1.4 fm^{-1}. We show also, as solid lines, fits to this interaction based upon the parametrization described by Eqs. (11). Good fits are obtained with only one free parameter per component; the parameters are listed in Table I. (Note that the scale factors S_i applied to the zero-density limit of the effective interaction are constrained to unity when reparametrizing a theoretical interaction; however, we find that the scale factors must be varied in order to reproduce the cross-section data for transitions with surface-peaked transition densities.) The density dependence of the real part of the central interaction can be described as an additive short-ranged repulsive interaction proportional to density. The density dependence of the imaginary part can be described by a Pauli blocking factor linear in k_F^2. The coefficient of k_F^2 turns out to be inversely proportional to energy, in agreement with the simple phase-space model of Clementel and Villi.[44]

Before applying the Ray interaction to scattering calculations, the original zero-density t matrix based upon the Lomon-Feshbach potential is replaced by the Franey-Love (FL) fit to nucleon-nucleon phase shifts. This procedure is similar to that used by Ray, who added the difference between the density-dependent and zero-density interactions to an interaction based upon the Arndt phase shifts.

C. Self-consistency

The calculated scattering observables involve integration over distorted waves in the initial and final states χ_i and χ_f. These distorted waves were generated from an optical potential computed from the fitted interaction in a self-consistent manner. Our first iteration uses distorted waves calculated from an optical potential computed from the theoretical interaction of Ray. Six parameters of the empirical interaction in Eqs. (11) are varied in a search routine that uses a least-squares optimization algorithm to fit the inelastic-scattering data. The fitted interaction is then used to compute a new optical potential and distorted waves. The fit of the interaction is performed again and the distorted waves iterated until the parameters of the interaction converge, generally within eight iterations. To improve the stability of the search procedure, the distorting potential is evaluated using parameters that represent the average of the previous two iterations. As noted above, an important component in the computation of an optical potential from the fitted interaction is the removal of the rearrangement contributions identified by Cheon, Takayanagi, and Yazaki.[42]

D. Selected transitions

In addition to the data reported here for transitions in ^{16}O, we obtained tables of proton inelastic-scattering data from ^{40}Ca at 500 MeV from Seth *et al.*[45] and from Lisantti *et al.*[46] From this set of data, we selected the following six transitions in ^{16}O: the 0_3^+ at 12.049 MeV, the 1_1^- at 7.117 MeV, the 2_1^+ at 6.917 MeV, the 2_3^+ at 11.521 MeV, the 3_1^- at 6.130 MeV, and the 4_1^+ at 10.353 MeV. In addition, we selected the following four transi-

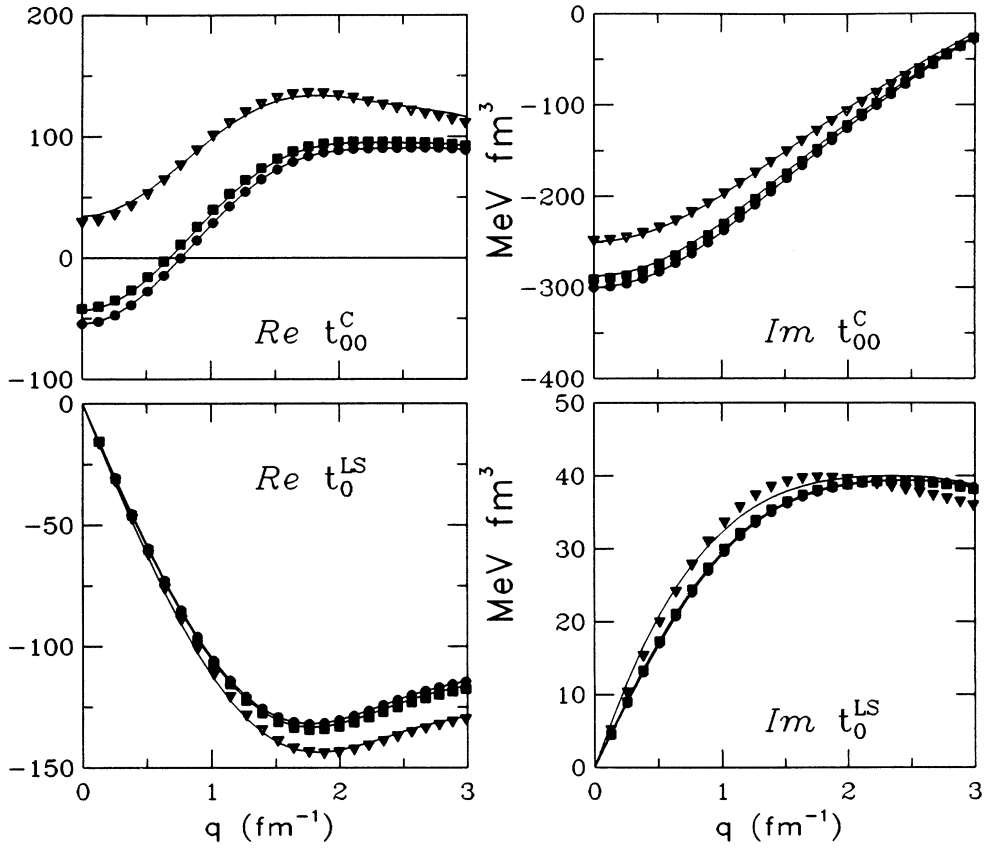

FIG. 1. Components of the isoscalar effective interaction of Ref. 4 for 500-MeV protons at three nuclear densities; $k_F=0.0$ fm^{-1} (circles), $k_F=0.7$ fm^{-1} (squares), and $k_F=1.4$ fm^{-1} (triangles). The solid lines are the results fitting an empirical interaction of the form given in Eqs. (11) to the theoretical interaction.

tions in ^{40}Ca: the 2_1^+ at 3.90 MeV, the 3_1^- at 3.74 MeV, the 3_2^- at 6.29 MeV, and the 5_1^- at 4.49 MeV. Of these transitions, the 2_1^+, 2_3^+, 3_1^-, and 4_1^+ states in ^{16}O and the 2_1^+, 3_1^-, and 5_1^- states in ^{40}Ca have surfaced-peaked transition densities and are thus coupled primarily to the low-density part of the effective interaction. The 0_3^+ and the 1_1^- states in ^{16}O have transition densities that peak in the nuclear interior and are thus coupled to the high-

TABLE I. Comparison of the parametrizations of effective interactions; the parameters S_i and b_i refer to Eqs. (11). The parentheses indicate that the associated parameter was held fixed to that value during the fitting process.

	Ret^C		Imt^C		Reτ^{LS}		Imτ^{LS}	
Interaction	S_1	b_1 (MeV fm^3)	S_2	d	S_3	b_3 (MeV fm^5)	S_4	b_4 (MeV fm^5)
Ray[a]	(1.00)	76.0	(1.00)	0.15	(1.00)	1.22	(1.00)	−1.92
EI-1[b]	1.26	121.1	0.84	−0.28	0.72	4.65	(1.00)	(−1.92)
EI-2[c]	0.82	236.1	0.93	−0.18	0.71	6.95	(1.00)	(−1.92)
EI-3[d]	0.87	199.5	0.88	−0.25	0.73	5.80	(1.00)	(−1.92)
EI-1A[e]	0.88	152.2	0.80	−0.30	0.73	5.14	(1.00)	(−1.92)
ALT-1[b]	1.26	122.3	0.83	(0.15)	0.70	4.96	(1.00)	(−1.92)
			$b_2=-126.5$ MeV fm^3					

[a]Reference 4.
[b]Fitted to ^{16}O data.
[c]Fitted to ^{40}Ca data.
[d]Fitted to both ^{16}O and ^{40}Ca data.
[e]Fitted to ^{16}O data with S_1 variation limited.

density part of the interaction. The 3_2^- state in ^{40}Ca has a double-lobed transition charge density, with one lobe in the high-density nuclear interior and one at the surface. Therefore, the selection of these ten transitions gives us sensitivity to the full spectrum of nuclear densities. We note that the spin-convection density discussed in Ref. 47 may contribute to the 0_3^+ transition near $q=1.5$ fm^{-1}. Although the cross-section data for this transition are not reproduced as accurately in this region, inclusion of data for the 0_3^+ transition did not significantly affect the form of the fitted interaction.

In addition to cross-section and analyzing-power distributions, available for all of the transitions of interest, distributions for a full set of spin observables are available for the 1_1^-, 2_1^+, and 3_1^- transitions in ^{16}O and some data for spin observables (see below) is available for the 3_1^- and 5_1^- transitions in ^{40}Ca.[34] It was hoped that these data for spin observables would be sufficient to determine the parameters for the Imτ^{LS} term, but this was not the case. It is also worth noting that essentially identical fits to the depolarization data are obtained whether or not these data are included in the fitting process.

IV. RESULTS

A. Interaction fitted to ^{16}O(p,p')

Calculations for the scattering of 500-MeV protons using either the impulse approximation (NRIA) based upon the Franey-Love t matrix (long dashes) or the local density approximation (LDA) based upon the Ray theoretical interaction (short dashes) are compared in Figs. 2–7 with the elastic- and inelastic-scattering data from ^{16}O. For transitions with surface-peaked transition densities ($2_1^+,2_3^+,3_1^-,4_1^+$), the NRIA describes the low-q cross-section data fairly well, but underpredicts the higher-q data. For transitions with interior-peaked transition densities (1_1^- and 0_3^+), the NRIA cross-section predictions fall well below the low-q data. These results are similar to those obtained at 318 MeV,[17] but should be contrasted with the situation for energies below 200 MeV,[15,16] for which the NRIA produces low-q cross sections which are much too strong for transitions with interior densities. For all states the NRIA distributions need to be pushed outward to describe the cross-section data for larger momentum transfer.

Analyzing powers calculated in the NRIA are systematically too large for low-momentum transfer and display oscillatory structures with variations that are both too rapid and too strong to describe the data adequately. This particular failure of the impulse approximation for the description of elastic-scattering spin observables at 500 MeV provided much of the early impetus for the development of the Dirac relativistic impulse approximation (DRIA).[20,48,49] Similarly, we find that the NRIA fails to describe the depolarization data for inelastic scattering. Most notably, NRIA calculations of D_{LS} and D_{SL} for the transition to the 3_1^- state predict a pro-

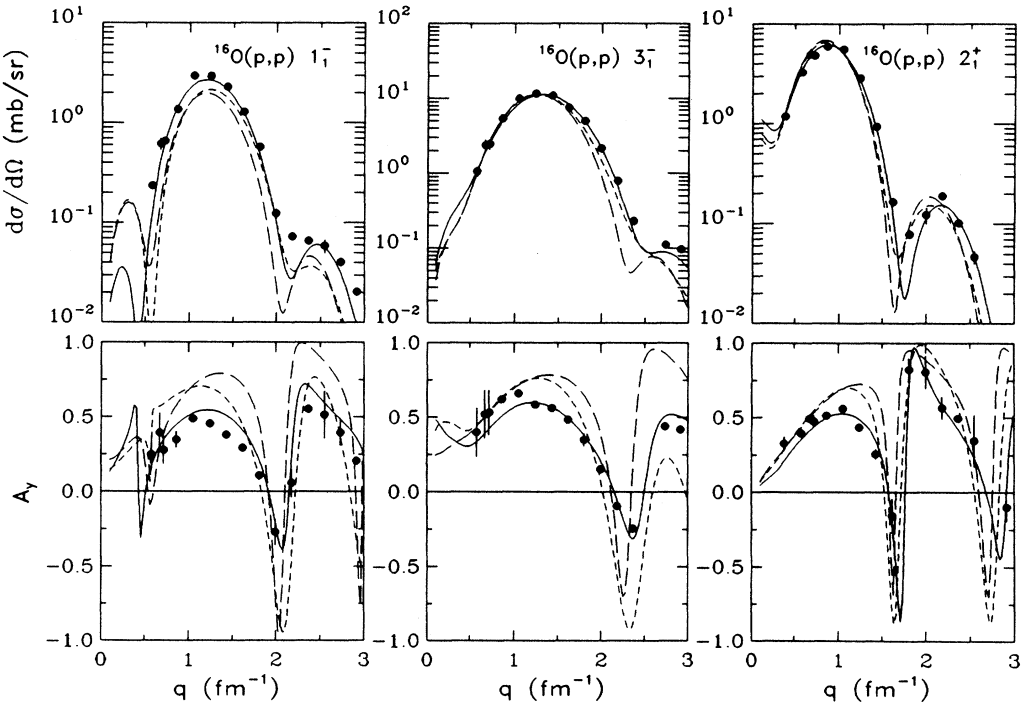

FIG. 2. Differential cross-section and analyzing-power data from proton inelastic scattering from ^{16}O to the 1_1^-, 2_1^+, and 3_1^- states are compared with NRIA t-matrix predictions (long dashes), LDA predictions with the Ray interaction (short dashes), and predictions with the empirical interaction (EI-1) fitted to the data (solid). Data for $q>2.7$ fm^{-1} are displayed, but were not included in the fits.

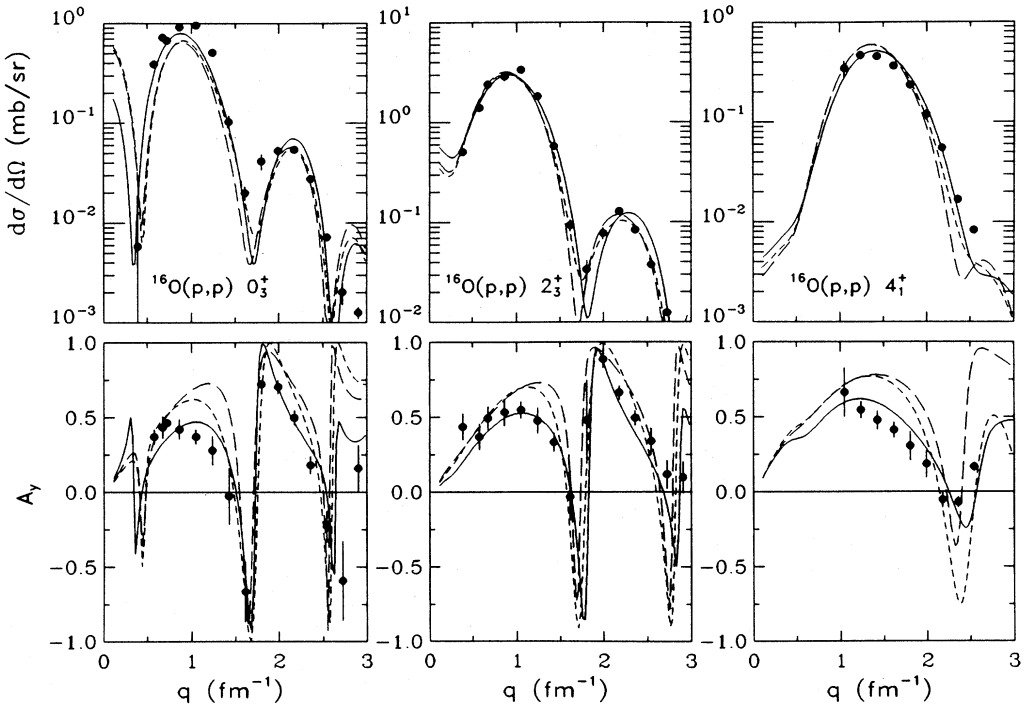

FIG. 3. Differential cross-section and analyzing-power data from proton inelastic scattering from ^{16}O to the 0_3^+, 2_3^+, and 4_1^+ states are compared with NRIA t-matrix predictions (long dashes), LDA predictions with the Ray interaction (short dashes), and predictions with the empirical interaction (EI-1) fitted to the data (solid). Data for $q > 2.7$ fm^{-1} are displayed, but were not included in the fits.

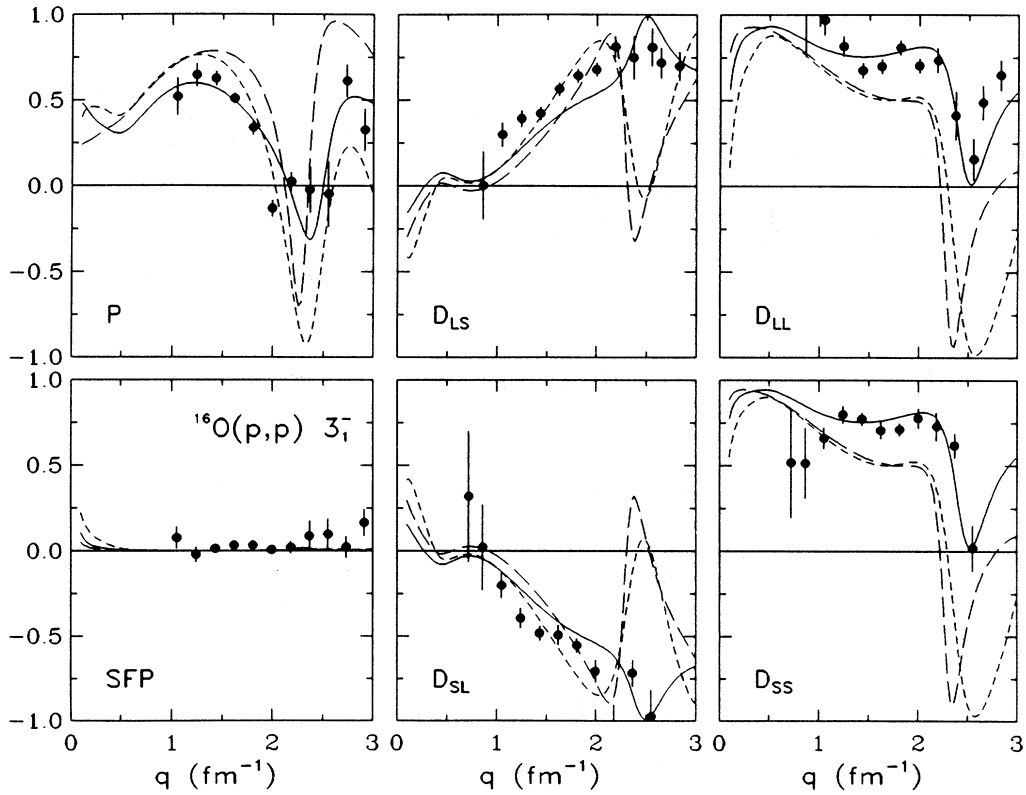

FIG. 4. Spin-observable data for the 3_1^- state of ^{16}O are compared with NRIA t-matrix predictions (long dashes), LDA predictions with the Ray interaction (short dashes), and predictions with the empirical interaction (EI-1) fitted to the data (solid). Data for $q > 2.7$ fm^{-1} are displayed, but were not included in the fits.

nounced structure near 2.5 fm^{-1} that is absent from the data.

Improvements provided by the density dependence of the Ray theoretical interaction are rather modest. These LDA calculations do provide a small enhancement of the high-q cross sections and a small suppression of the low-q analyzing powers, but fail to enhance the peak cross sections for transitions with interior densities. Similarly, the changes in the calculations of the depolarization parameters are not large enough. Although the discrepancies between the calculations in the NRIA and the data are greater for transitions with densities that probe the interior of the nucleus, suggestive of a density-dependent effect, the Pauli blocking and dispersive effects included in the Ray theoretical interaction do not have a sufficiently strong dependence on the density.

Therefore, we have fitted the parameters of an empirical effective interaction to inelastic-scattering data for five transitions in ^{16}O simultaneously, including cross-section and analyzing-power data for transitions to the 1_1^-, 2_1^+, 2_3^+, 3_1^-, and 4_1^+ states and depolarization data for transitions to the 1_1^-, 2_1^+, and 3_1^- states. Six parameters of the empirical effective interaction were varied with the first iteration starting from parameters derived by fitting the model to the Ray theoretical interaction; these initial parameters (see Table I) were used to generate both the optical potentials and empirical interaction. Eight iterations were required to obtain self-consistency between the distorting potentials and inelastic interaction. The parameters of the resulting empirical effective interaction, labeled EI-1, are compared in Table I with the parameters which result from fitting the model to the Ray theoretical interaction. We note that the empirical interaction has a much stronger dependence on density than the Ray interaction.

We find that the empirical effective interaction EI-1 provides an excellent global fit to all of the ^{16}O data displayed in Figs. 2–7. Cross sections for transitions with interior densities are enhanced by as much as 50%, in good agreement with the data. Cross sections for other transitions also receive the requisite enhancements at larger momentum transfer. Analyzing-power distributions are dramatically and uniformly improved for all transitions considered. In particular, the forward-angle analyzing powers that marked the most significant failure of the NRIA are very well described by the empirical effective interaction in a nonrelativistic framework. Perhaps most striking is the quality of the fit to the depolarization data for the transition to the 3_1^- state of ^{16}O. With the empirical effective interaction, the D_{SL} and D_{LS} distributions are described very well for the entire range of the data, including the features near 2.5 fm^{-1}, which

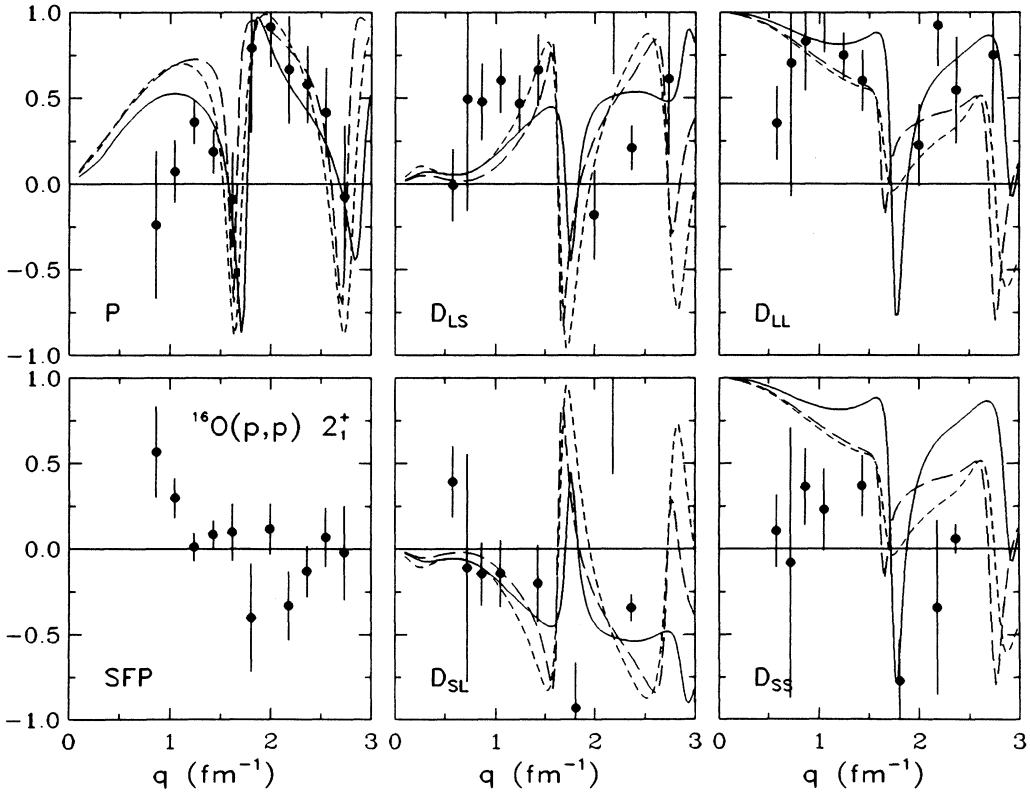

FIG. 5. Spin-observable data for the 2_1^+ state of ^{16}O are compared with NRIA t-matrix predictions (long dashes), LDA predictions with the Ray interaction (short dashes), and predictions with the empirical interaction (EI-1) fitted to the data (solid). Data for $q > 2.7$ fm^{-1} are displayed, but were not included in the fits.

neither the NRIA nor the Ray theoretical interaction described.

It is worth noting that the depolarization data for the 3_1^- state, which is the strongest and most collective of the transitions observed, satisfy the same symmetry relations [Eq. (1)], as do the elastic data. Although not strictly required, this behavior is expected for collective excitations driven by the matter density and for which transverse form factors and spin-flip contributions are negligible. Although the error bars are much larger for the weaker 1_1^- state, these data do seem to show significant differences, $D_{SS} \neq D_{LL}$ and $D_{SL} \neq -D_{LS}$, which may be due to non-negligible spin-flip probability. Although insignificant for cross-section and analyzing-power calculations, F_T^2 is observed in electron scattering to reach about 1% of F_L^2 near the peak of the 1_1^- form factor. Unfortunately, acquisition of data with sufficient statistical precision to verify these apparent deviations from collective behavior would have required considerably more beam time.

An important test of the self-consistency procedure is provided by the elastic-scattering data, which were not included in the fitting procedure. Predictions for elastic scattering from ^{16}O and ^{40}Ca based upon the empirical effective interaction EI-1, the NRIA, and the Ray interaction are compared with the data in Fig. 7. The density dependence of the Ray interaction is not sufficient to produce the enhancement of the high-q elastic cross section needed to describe the data for both nuclei. This effect is accurately described by the empirical effective interaction. Similarly, although the Ray interaction suppresses low-q analyzing powers and does turn around the classic upward cusp in the NRIA calculation for the ^{40}Ca analyzing power at about 1.0 fm^{-1}, the substantially stronger density dependence of the empirical effective interaction is needed to obtain quantitative agreement with the data using a nonrelativistic model. In fact, the analyzing-power predictions provided by the empirical effective interaction are superb, more accurate than any current microscopic model, relativistic or nonrelativistic.

Note that use of the rearrangement factor $(1+\rho\,\partial/\partial\rho)$ is crucial to the success of the self-consistency procedure. If this factor is omitted, the density-dependent coefficients fitted in the first iteration are approximately twice as strong and elastic cross sections calculated from these larger coefficients are about an order of magnitude stronger than the data for high q. Moreover, the iteraction procedure does not converge upon a self-consistent solution if the rearrangement factor is omitted. Only when a relationship of this type between elastic and inelastic interactions is employed can a self-consistent solution be reached. Therefore, the success of the present

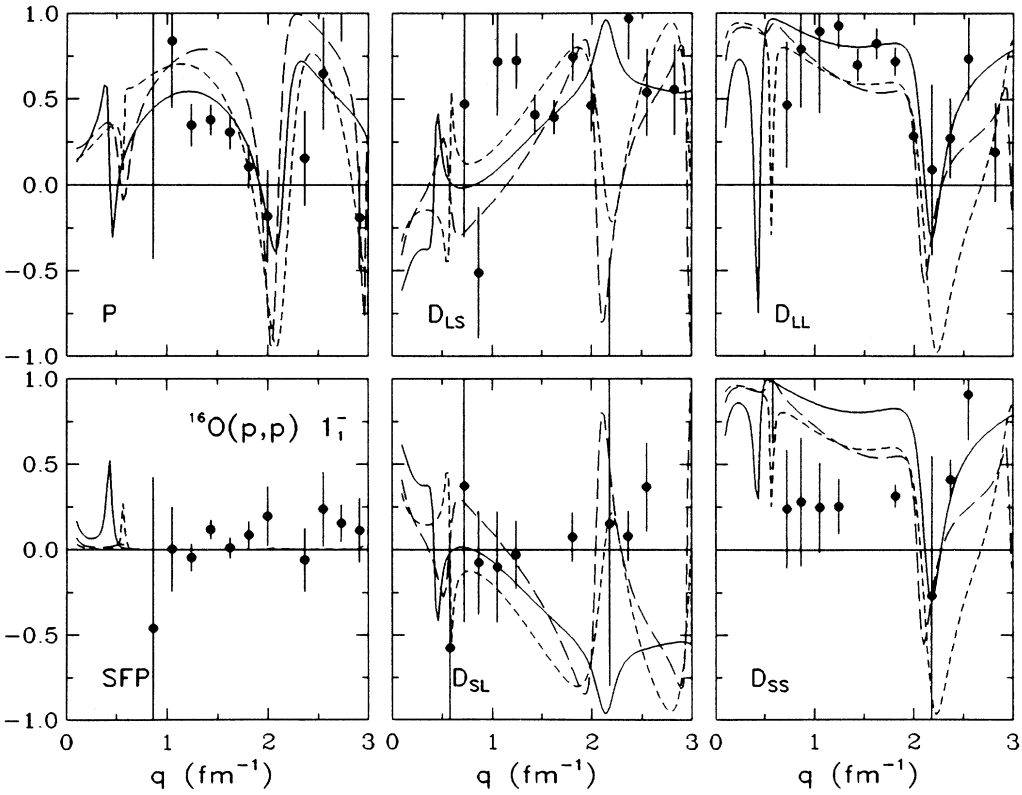

FIG. 6. Spin-observable data for the 1_1^- state of ^{16}O are compared with NRIA t-matrix predictions (long dashes), LDA predictions with the Ray interaction (short dashes), and predictions with the empirical interaction (EI-1) fitted to the data (solid). Data for $q > 2.7$ fm^{-1} are displayed, but were not included in the fits.

model is strong evidence for the accuracy of the Cheon rearrangement factor. However, it appears that the density dependence for elastic scattering may still be slightly too strong. Similar results were also obtained at 318 MeV, for which the tendency to overestimate high-q elastic cross sections was somewhat greater. These observations suggest that a minor modification of this relationship between elastic and inelastic interactions may be needed.

B. Comparison with other nuclei

If the local-density approximation is valid, the effective interaction should depend upon density, but not nuclear species. Thus we can test the empirical effective interaction by comparing calculations performed with this interaction (EI-1, fitted to data for ^{16}O) to data for transitions in ^{40}Ca. The results of this test are shown for elastic scattering and for the 2_1^+, 3_1^-, 3_2^-, and 5_1^- transitions of ^{40}Ca as the solid lines in Figs. 7–10. For comparison, calculations using either the t matrix (NRIA, long dashes) or the Ray theoretical interaction (LDA, short dashes) are shown also. The predictions of the NRIA show the same deficiencies for ^{40}Ca as were noted above for transitions in ^{16}O; the improvements provided by the Ray theoretical interaction calculations are again modest.

The empirical effective interaction gives substantial improvements over the Ray theoretical interaction calculations for inelastic scattering from ^{40}Ca. As for ^{16}O, the cross-section distributions are shifted toward larger q and the analyzing powers are reduced in amplitude, in good agreement with the data. For the 3_1^- transition, we find that the strong oscillation in D_{SL} and D_{LS} predicted near 1.5 fm^{-1} by the NRIA, and absent from the data, is muted by the empirical interaction. At lower-momentum transfers, D_{LL} and D_{SS} are increased and describe the data better. Therefore, we conclude that the local-density-approximation description is consistent with the data, but that the dependence on density is stronger than provided by existing nonrelativistic theoretical interactions. At the present level of accuracy, all of the data for normal-parity excitations (including elastic scattering) of both ^{16}O and ^{40}Ca can be described by the same effective interaction without need of A-dependent multistep processes.

As an additional test, we have fitted the parameters of the empirical interaction to the cross-section and analyzing-power data for the transitions to the 2_1^+, 3_1^-, 3_2^-, and 5_1^- states and the depolarization data for the 3_1^- and 5_1^- states of ^{40}Ca simultaneously, starting from the parameters of interaction EI-1. Finally, we fitted the parameters of the interaction to the combined ^{16}O plus ^{40}Ca data sets. The parameters from the fit to the ^{40}Ca data set are labeled EI-2, and the parameters from the fit to

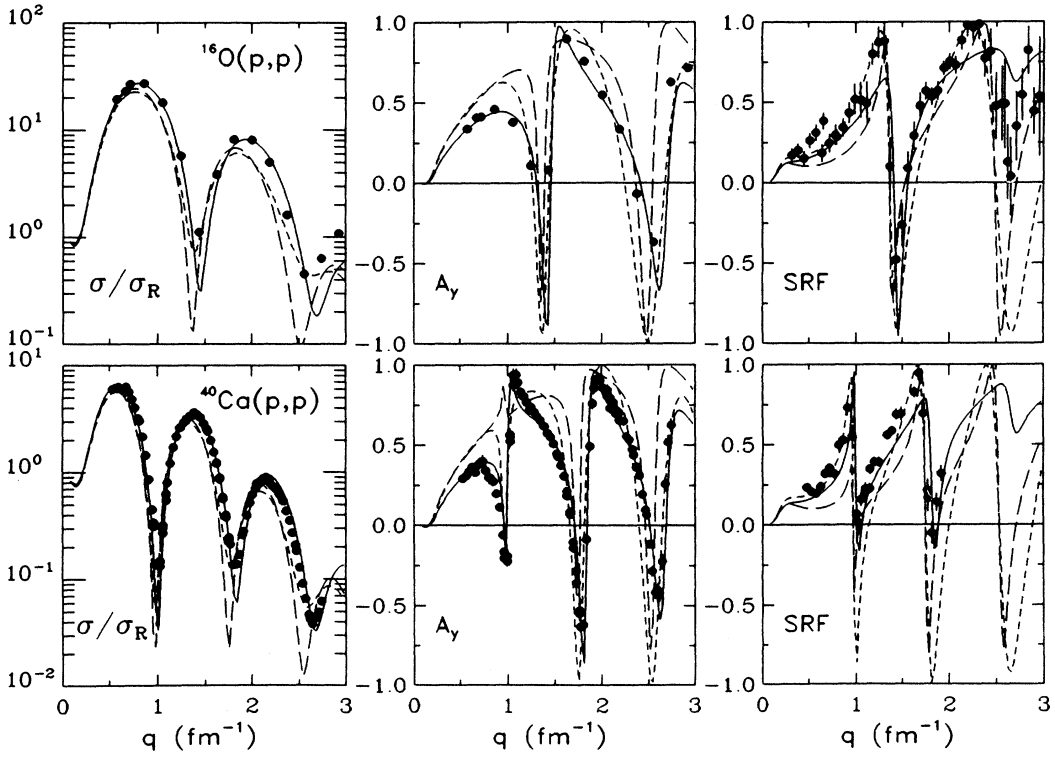

FIG. 7. Differential cross-section (presented as the ratio to Rutherford to enhance detail), analyzing-power, and spin-rotation function (SRF) data for proton elastic scattering from ^{16}O and ^{40}Ca at 500 MeV are compared with three sets of predictions. The curves correspond to the NRIA t-matrix predictions (long dashes), LDA predictions with the Ray interaction (short dashes), and predictions with the empirical interaction (EI-1) fitted to the ^{16}O inelastic-scattering data (solid).

the combined data set are labeled EI-3 and are compared with the previous results in Table I. For the fit to the combined data set, a subset of the ^{40}Ca data plotted in these figures was used so as to weight the contributions to χ^2 from ^{16}O and ^{40}Ca roughly equivalently. With only 6 free parameters, an excellent fit to 46 distributions among 10 transitions in 2 nuclei is achieved (EI-3). We find that the quality of the predictions for calculations with each of the three fitted interactions is almost identical and nearly indistinguishable to the eye; however, as can be seen in Table I, the parameters for the three interactions are significantly different. The largest effect observed when the ^{40}Ca data set is included in the fit is that the scale factor for the $\mathrm{Re}t^C$ term is reduced and the dependence on density is increased. Since increased absorption reduces the sensitivity to the nuclear interior, it is likely that the ^{40}Ca data set does not determine the effective interaction as well as the ^{16}O data set. Nevertheless, as noted above, the ^{40}Ca data are described well by the interaction fitted to the ^{16}O data (EI-1) and calculations performed with interaction EI-2 provide a good description of the observables for transitions in ^{16}O, although, as measured by χ^2, the description of the ^{16}O data is better for the calculations with either interaction EI-1 or EI-3. Therefore, we conclude that the data are consistent with density-dependent effective interactions that are independent of nuclear species.

As a final test of the A independence of the interaction and of the local-density hypothesis, we compare elastic-scattering predictions based upon the EI-1 interaction with data[50,51] for ^{12}C and ^{208}Pb in Fig. 11. These calculations use densities constructed by Ray and Hoffman[52] based upon proton densities from electron scattering and neutron densities obtained by adding DDHFB predictions[53] of the neutron-proton density difference to experimental proton densities. We observe that, to very good accuracy, the interaction fitted to inelastic-scattering data from ^{16}O describes elastic-scattering data from nuclei near the extremes of the mass range. The largest deficiencies are observed for the cross-section calculations at larger q where the fitted interaction appears to have a somewhat too strong density dependence, particularly for light nuclei. The empirical interaction fills up the first three peaks in σ/σ_R for ^{208}Pb considerably better than the NRIA or Ray interactions. The improvement in the analyzing-power calculation for ^{208}Pb is particularly impressive and remedies the discrepancy identified by Ray[4] as the most glaring failure of his density-dependent interaction. The ability of an interaction fitted to inelastic scattering from ^{16}O to reproduce data for elastic scattering by ^{208}Pb strongly supports the accuracy of the empirical effective interaction and the applicability of the local-density approximation.

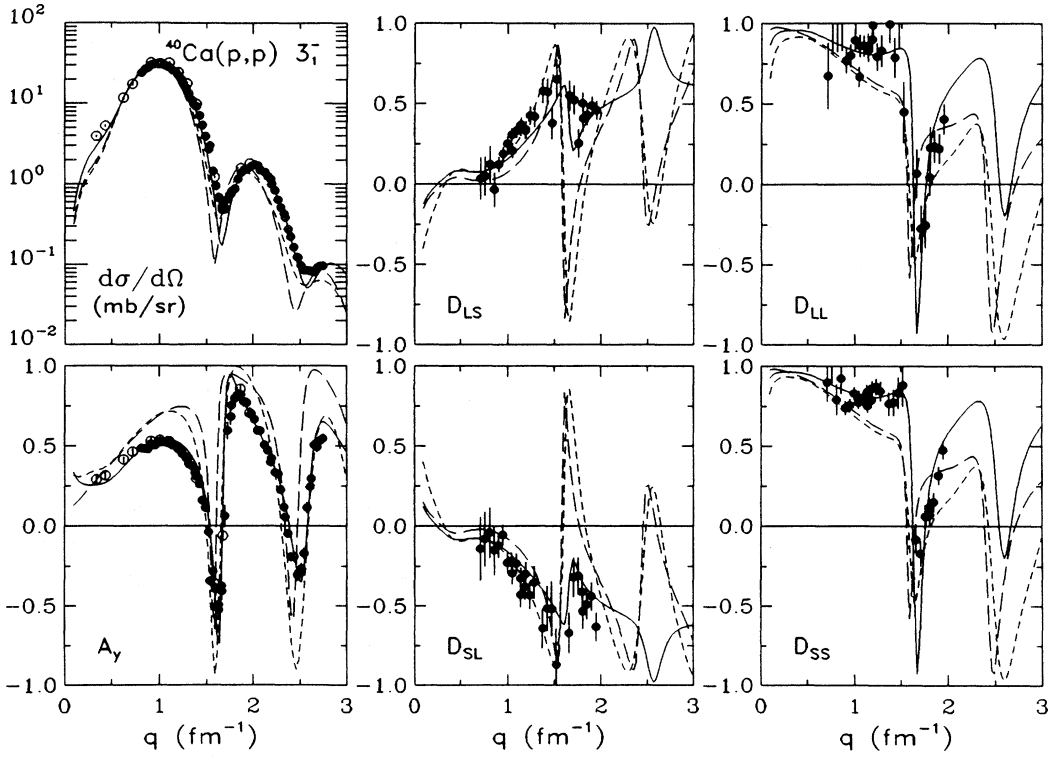

FIG. 8. Differential cross-section, analyzing-power, and spin-observable data for the 3^-_1 transition in ^{40}Ca are compared with NRIA t-matrix predictions (long dashes), LDA predictions with the Ray interaction (short dashes), and predictions with the empirical interaction (EI-1) fitted to ^{16}O data (solid). Cross-section and analyzing-power data are shown as solid circles for Ref. 45 and open circles for Ref. 46. Data for depolarization coefficients are taken from Ref. 34.

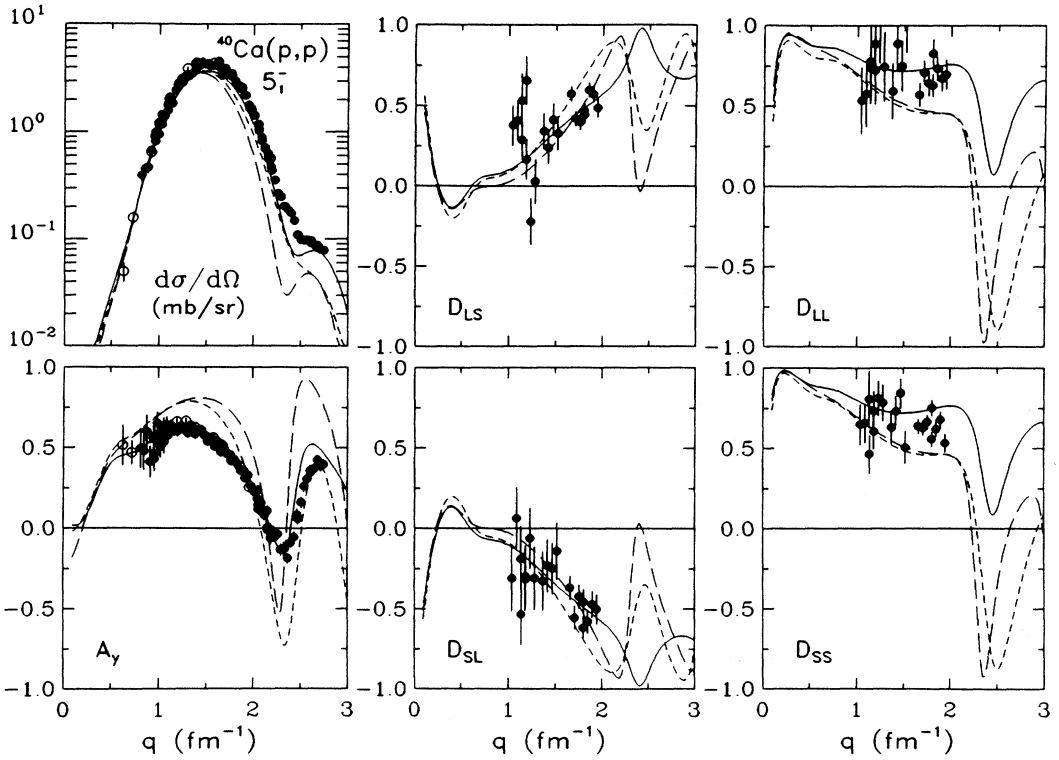

FIG. 9. Differential cross-section, analyzing-power, and spin-observable data for the 5_1^- transition in ^{40}Ca are compared with NRIA t-matrix predictions (long dashes), LDA predictions with the Ray interaction (short dashes), and predictions with the empirical interaction (EI-1) fitted to ^{16}O data (solid). Cross-section and analyzing-power data are shown as solid circles for Ref. 45 and open circles for Ref. 46. Data for depolarization coefficients are taken from Ref. 34.

C. Empirical effective interaction for 500 MeV

In this section we attempt to interpret the parameters of the empirical effective interaction (EI-1) in the context of the nonrelativistic impulse approximation. An alternative interpretation based upon the relativistic impulse approximation is presented in Sec. V.

In Figs. 12 and 13 we compare the optical potentials for ^{16}O and ^{40}Ca derived from the t matrix (long dashes), the Ray theoretical interaction (short dashes), and the empirical effective interaction (EI-1) (solid lines). All three calculations give similar results for the spin-orbit potentials and for the central potentials at large radii, where the density is small. In the interior we find that the density-dependent repulsive core in the Ray theoretical interaction changes the sign (with respect to the t matrix) of the real central potential and that this effect is nearly twice as large with the empirical interaction. More surprisingly, whereas Pauli blocking in the Ray interaction suppresses the absorptive potential in the interior, the empirical effective interaction produces a modest enhancement of the imaginary central potential. This effect would have been even larger had the scale factor S_2 been closer to unity. These changes, predicted from fits to inelastic-scattering data, are also required to reproduce the elastic-scattering data.

The parameters of the empirical effective interaction (EI-1) are compared with those of the theoretical interaction in Table I. The most striking difference between

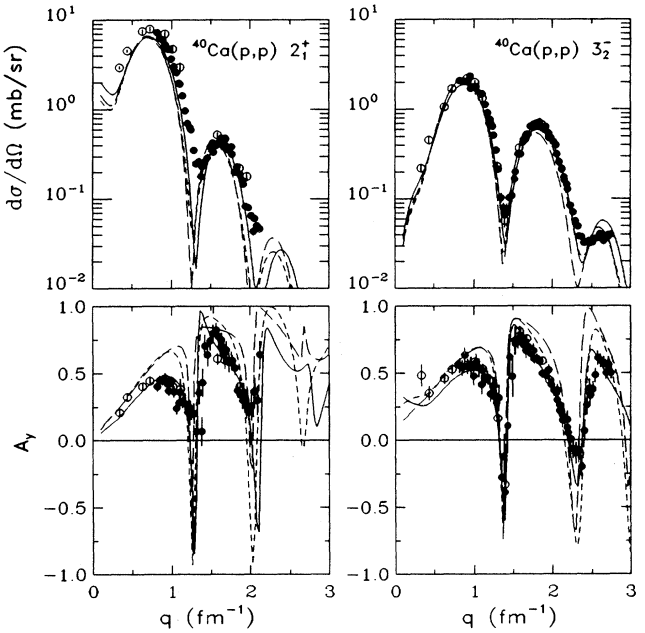

FIG. 10. Differential cross-section and analyzing-power data for the 2_1^+ and 3_2^- states in ^{40}Ca are compared with NRIA t-matrix predictions (long dashes), LDA predictions with the Ray interaction (short dashes), and predictions with the empirical interaction (EI-1) fitted to ^{16}O data (solid). Cross-section and analyzing-power data are shown as solid circles for Ref. 45 and open circles for Ref. 46.

these models is found in the $\mathrm{Im}t^C$ component. As found for lower energies, the strength of this component is reduced by a factor of about 0.8; however, instead of further damping at higher densities, the negative sign of the fitted *Pauli blocking* parameter shows that the empirical interaction becomes stronger with increasing density. This behavior is contrary to predictions based upon the Ray theoretical interaction and is opposite to the damping exhibited by empirical interactions fitted to data for energies below 300 MeV. We have attempted many alternative fits in which (1) this parameter was constrained to be positive, (2) the damping term was replaced with either a delta function or a Yukawa term, (3) different selections of data were fitted, (4) different parameters were varied, or (5) different starting conditions were employed, but in all cases we find that a good fit to the data can be obtained only when the essential characteristics of the current result are retained, namely, the reduced zero-density strength and its enhancement with increasing density. Therefore, we conclude that these general properties of this component are unambiguous, at least within the context of the NRIA.

Some insight into the meaning of this result is provided by the observation that the empirical damping parameter changes sign near the pion-production threshold. Fits to data from ^{16}O and ^{40}Ca at 318 MeV also result in a negative, albeit small, value for this parameter and the description of inelastic-scattering data for 650- and 800-MeV protons also suggest a negative value. For energies below 200 MeV, this parameter obeys the E^{-1} energy dependence predicted by simple Pauli blocking of the phase space for quasifree scattering, which dominates absorption at lower energies.[44] However, the sign change near 300 MeV suggests that absorption is enhanced at high densities when the pion-production channel is open. The fact that the magnitude of this effect increases between 318 and 500 MeV is consistent with the increased absorption into that channel.

The density dependence of $\mathrm{Im}t^C$ in the theoretical interaction constructed by Ray continues to follow the E^{-1} energy dependence throughout the energy region $300 < E < 800$ MeV. Phase-space blocking evidently dominates this calculation despite its inclusion of inelasticity; however, recent calculations show that off-shell effects can have a substantial effect upon nucleon scattering even at 500 MeV.[54,55] These effects can be expected to depend strongly upon the model for the nucleon-nucleon interaction. Perhaps Fermi averaging over off-shell momenta can produce a large change in the inelasticity in the nuclear medium. Further theoretical effort will be required to clarify these possibilities and to explain the phenomenological results.[56] In the meantime some of the effects are implicitly incorporated into the effective interaction fitted to data.

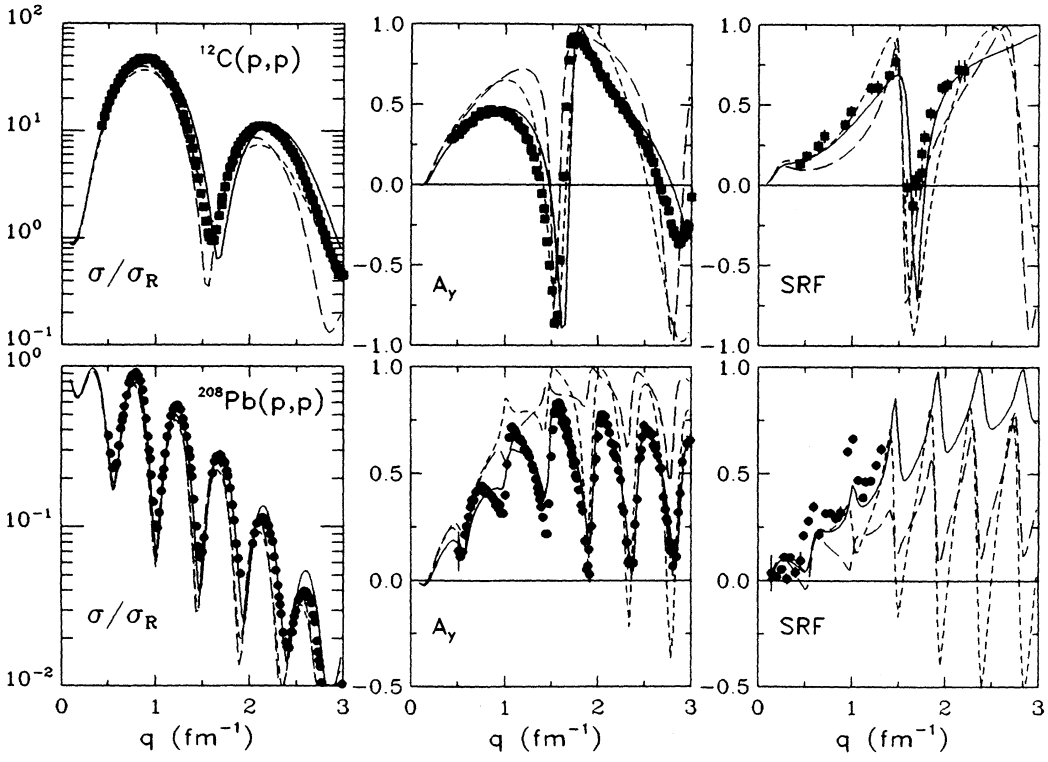

FIG. 11. Differential cross-section (presented as the ratio to Rutherford to enhance detail), analyzing-power, and spin-rotation function (SRF) data for proton elastic scattering from ^{12}C and ^{208}Pb at 500 MeV are compared with three sets of predictions. The curves correspond to the NRIA t-matrix predictions (long dashes), LDA predictions with the Ray interaction (short dashes), and predictions with the empirical interaction (EI-1) fitted to the ^{16}O inelastic-scattering data (solid).

The density dependence of the real part of the central interaction is related more simply to the Ray theoretical interaction and to the results for lower energies. Based upon the theoretical interaction calculations, we can expect the strength of the repulsive core to increase slowly with energy; however, the value of this parameter (S_1) depends upon the free interaction used in the phenomenology. For energies below 200 MeV, better fits to the data were obtained using the PH interaction at zero density than were obtained using the FL t matrix, despite the fact that the PH model of the G matrix does not reduce to the t matrix at low density. Most notably, the real central component of the low-density PH interaction is stronger for large momentum transfer than the corresponding component of the t matrix. Hence, if the FL interaction is used as the basis of the empirical interaction, the S_1 and b_1 parameters are both increased relative to those obtained with the zero-density PH interaction, so that the resulting fitted interaction is nearly independent of the choice of free interaction. In Ref. 11 it was suggested that the difference between the t matrix and PH interaction at low density is related to off-shell properties of the nucleon-nucleon interaction that are incorporated by the Brieva and Rook[7] prescription for deriving a local interaction from matrix elements involving the correlated-pair wave function. This effect appears to persist at 500 MeV. Finally, we observe that the parameters which describe the density dependence of the real part of the spin-orbit interaction are almost independent of projectile energy. Also, at 500 MeV these parameters are relatively insensitive to the form of the parametrization of the central components or to the data set fitted.

D. Alternative parametrizations

A second starting point for the fit to the ^{16}O data was obtained by performing a manual scan through each of the six parameters individually to find a "best value" for that parameter. This was accomplished by stepping each parameter through a specified grid of values while allowing the other five parameters to vary. The *best value* for each parameter was chosen as that which minimized the deviations between the calculations and data. This method yielded a starting point for the fitting procedure which had both smaller deviations (χ^2) than the Ray theoretical interaction and parameters more consistent with the results obtained at lower energies. However, starting from these parameters, the fitting procedure generally converged to parameters similar to those for interaction EI-1, unless restrictions were placed on the fitting procedure. The interaction EI-1 appears to correspond to a broad local minimum in chi-square space; by

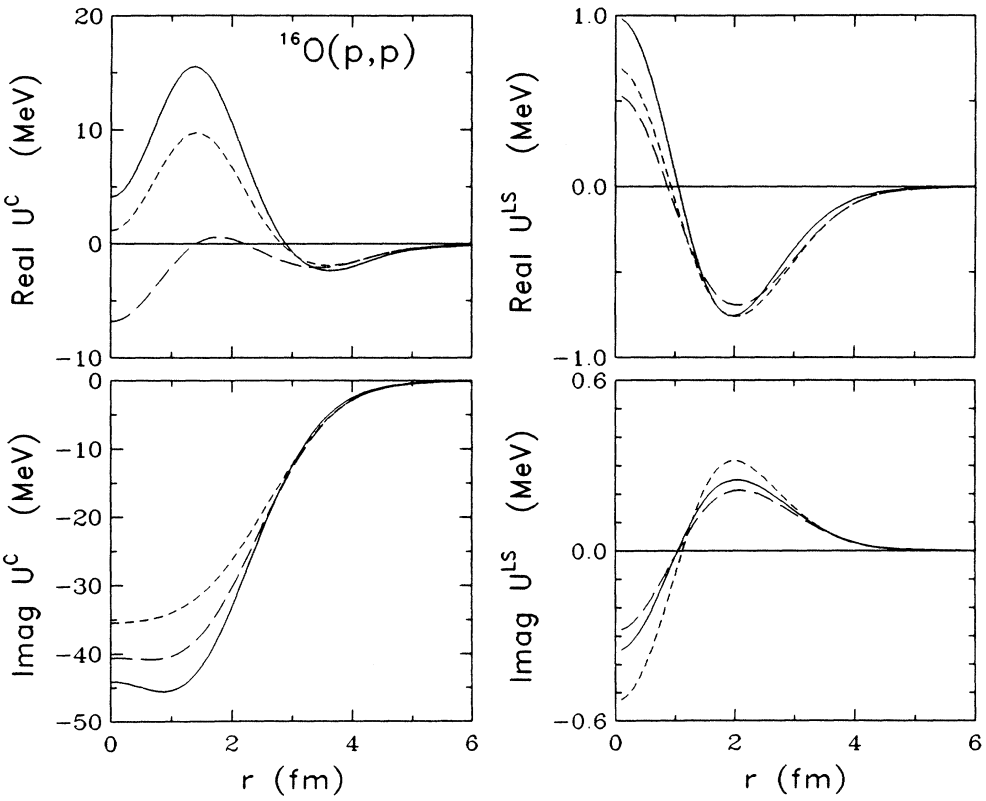

FIG. 12. Components of the optical potential for 500-MeV protons on ^{16}O. The long-dashed lines use the NRIA interaction of Ref. 2, the short-dashed lines use the theoretical interaction of Ref. 4, and the solid lines use the empirical interaction fitted to the ^{16}O data (EI-1).

keeping the search out of this minimum, convergence in another, deeper minimum occurs. The restriction we chose was to limit the step size for one of the parameters (S_1) so that the first step would not take the search into the area of the broad minimum. The parameters that result from this search are listed in Table I as EI-1A. The chi square associated with interaction EI-1A is smaller than that for EI-1. In addition, the scale factor for the Ret^C term is now less than 1, in agreement with our prejudices from similar work at lower energies.[15,16] The expense for this reduced scale factor is a 30% increase in the density dependence for this term; the other four parameters differ by less than 10% from their values for interaction EI-1.

This second solution EI-1A points outs the ambiguity which exists in the determination of the real part of the central interaction. The correlation between the parameters S_1 and b_1 in the fitting process is large, and a tradeoff between them can leave the general features of the interaction unaffected; one can compensate for a decrease in the strength of the low-density part of Ret^C by increasing the high-density part. This effect of reducing the scale factor and increasing the dependence on density was observed also when the ^{40}Ca data set was included in the fitting process (EI-2, EI-3); however, the increase in the b_1 parameter is much less for EI-1A than for EI-2 or EI-3. In Fig. 14 we compare the density and momentum transfer dependencies of the interactions EI-1 and EI-1A. As stated above, only the Ret^C component shows much difference; there are modest differences in Imt^C at low q and in Ret^{LS} at high q. For the Ret^C component the differences show both a density and momentum transfer dependence; at larger values of q, the EI-1A interaction is approximately 30 MeV fm^3 weaker than the EI-1 interaction at all densities, while at low q, EI-1 is stronger by about 25 MeV fm^3 at low density and is weaker by 60 MeV fm^3 at high density.

A useful method for comparing the effects of these differences on the scattering observables is to calculate the plane-wave impulse approximation (PWIA) analyzing power and *matter interaction* $|\tilde{t}_M|^2$, defined to be

$$|\tilde{t}_M(q)|^2=|\tilde{t}^C(q)|^2+|\tilde{t}^{LS}(q)|^2 . \tag{12}$$

For normal-parity transitions in the plane-wave limit,

$$\sigma(q)\sim|\tilde{\rho}_J(q)|^2|\tilde{t}_M(q)|^2 , \tag{13a}$$

$$A_y(q)\sim\mathrm{Im}\{[t^C(q)][t^{LS}(q)]^*\}/|\tilde{t}_M(q)|^2 , \tag{13b}$$

where ρ_J is the isoscalar matter transition density. Examining the third column of Fig. 14, we observe that despite the differences in the components of the interactions EI-1 and EI-1A, the matter interactions and analyzing powers show significant differences only at large q.

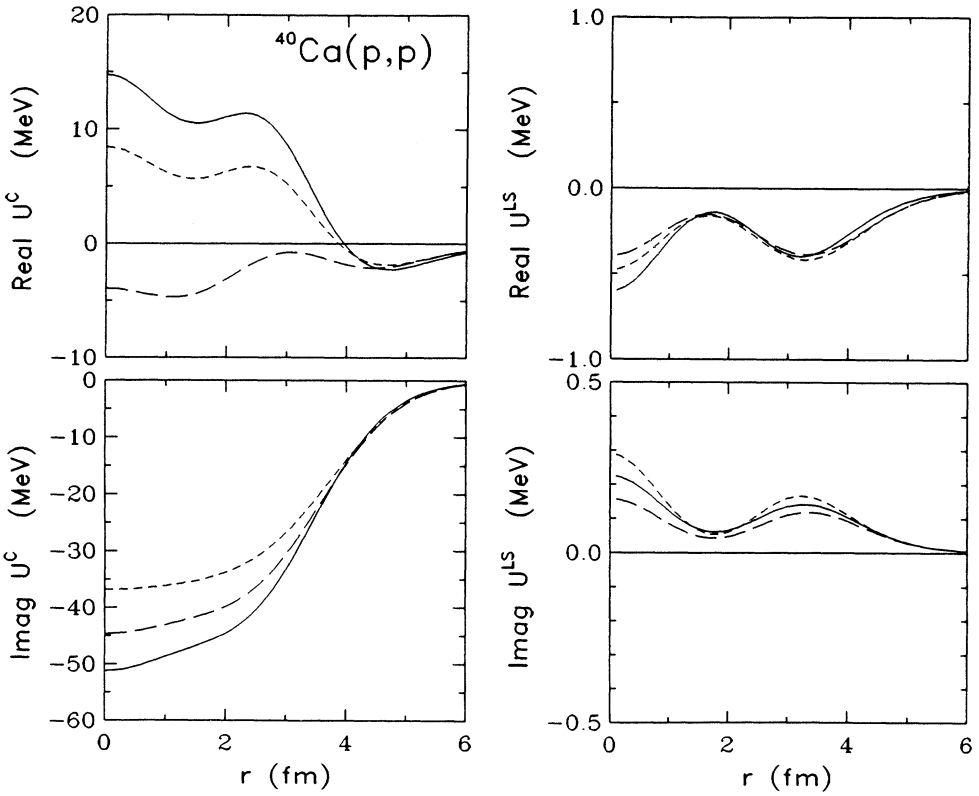

FIG. 13. Components of the optical potential for 500-MeV protons on ^{40}Ca. The long-dashed lines use the NRIA interaction of Ref. 2, the short-dashed lines use the theoretical interaction of Ref. 4, and the solid lines use the empirical interaction fitted to the ^{16}O data (EI-1).

The matter interaction EI-1A is seen to be weaker at large q by about 20%, which will reduce the cross section and increase the analyzing power.

Barlett *et al.*[57] investigated medium modifications to the nucleon-nucleon isoscalar interaction by deducing empirical effective interactions from folding model analyses of $\vec{p}$+nucleus elastic scattering at 500 MeV incident proton energy. The general form of the empirical density dependence that they used for each term in the interaction was

$$t(q,\kappa_F)=(s+b\kappa_F^3)t(q,0)\ . \tag{14}$$

With this form they fitted elastic-scattering observables for several nuclei to extract s and b. We calculated inelastic-scattering observables using both their elastic-scattering interaction and an interaction obtained by applying the rearrangement factor given by Eq. (9); neither of these calculations provided good descriptions of the inelastic-scattering observables. We then attempted to fit the inelastic data by varying the parameter s and b in Eq. (14). All attempts to fit the data using this form of the density dependence were vastly inferior to the fits obtained with the form given in Eqs. (11). By applying a multiplicative factor to each component of the effective interaction, the Barlett form does not include the short-range repulsive core required to describe the data accurately. Also, without the benefit of inelastic transition densities concentrated in the high-density interior, it is difficult to extract the density dependence of the interaction from elastic-scattering data alone.

A fit to the data as good as that presented herein can be achieved with a slightly different form for the parametrization of the imaginary central interaction. The function

$$\mathrm{Im}t^C(q,\kappa_F)=(S_2-d\kappa_F^2)\mathrm{Im}t^C(q,0)+b_2\kappa_F^2 Y(q/\mu_2) \tag{15}$$

will have an ambiguity if $\mathrm{Im}t^C(q,0)$ and $Y(q/\mu_2)$ have similar dependencies upon q; then only the combination $[b_2-d\ \mathrm{Im}t^C(0,0)]$ can be determined uniquely. In fact, we find that if we choose $\mu_2=\mu_1=2.0$ fm^{-1}, then this condition is satisfied and equivalent fits to the data are found by varying b_2 instead of d. Hence we are free to assume that the Pauli blocking parameter d continues to follow the expected E^{-1} behavior, but that b_2 increases with energy. The b_2 parameter can then be interpreted either as a manifestation of virtual $N\bar{N}$ pairs or as enhanced absorption, pending the development of a more complete theoretical description of medium modifications in this energy regime. The value of the parameters that result from a fit to the ^{16}O data set with this form for $\mathrm{Im}t^C$ are listed in Table I as ALT-1. As can be seen, a rather substantial enhancement to $\mathrm{Im}t^C$ from the b_2 term is required to offset the Pauli blocking term d. In fact,

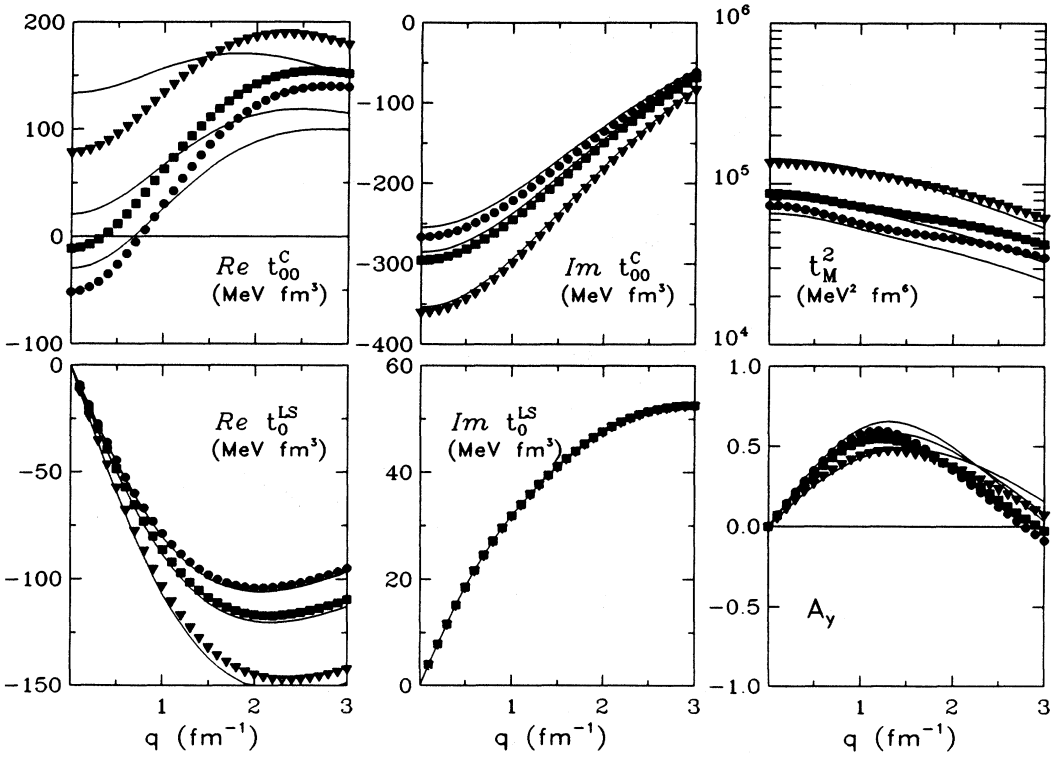

FIG. 14. Components of the effective interaction, matter interactions, and analyzing powers in plane-wave approximation for the empirical interactions EI-1 and EI-1A at three nuclear densities. The solid lines are the interaction EI-1A and the symbols are the interaction EI-1 at $k_F=0.6$ fm^{-1} (circles), $k_F=1.0$, fm^{-1} (squares), and $k_F=1.4$ fm^{-1} (triangles).

since $\mathrm{Im}t^C(0,0) \approx -300$ MeV fm^3, we would predict a value of $b_2 \approx -(0.28+0.15)300$ MeV fm$^3 \approx -129$ MeV fm^3 would produce an effective interaction equivalent to EI-1, in agreement with this fitted value.

V. DISCUSSION

A. Comparison with the relativistic impulse approximation

It is instructive to compare the optical potentials produced by the empirical interaction with the "Schrödinger-equivalent" potentials derived from the relativistic optical potential. This comparison is made for ^{40}Ca in Fig. 15, in which the dashed lines represent the NRIA and the circles the IA2 results of Ottenstein, Wallace, and Tjon.[5] The differences between these two sets of potentials may be attributed, in the Dirac model, to the effect of virtual $N\bar{N}$ pairs;[23] when reduced to Schrödinger form, this effect is observed as primarily a short-ranged repulsive interaction.[5] The solid lines in Fig. 15 are the optical potential derived from the empirical interaction (EI-1); apparently, the density dependence due to pair contributions is very similar to the empirical medium modifications fitted to inelastic scattering data.

Note that the NRIA potentials of Ottenstein, Wallace, and Tjon differ somewhat from our NRIA potentials; part of this difference occurs because they used the Dirac-Hartree wave functions of Horowitz and Serot,[58] while we used charge densities from electron scattering. Other differences occur because they used the phase shifts of Ref. 27, while we used the FL t matrix.[2] Nevertheless, these two versions of the NRIA produce essentially identical predictions of elastic scattering.

Calculations of elastic scattering from ^{16}O and ^{40}Ca based upon our empirical effective interaction (EI-1) and the Schrödinger-equivalent IA2 potentials are compared with the data in Fig. 16. In most respects our results provide a slightly more accurate description of the elastic-scattering data than does the IA2 model. In addition, we compare our calculations for ^{12}C with those of Ref. 50 based upon the early RIA model of McNeil, Ray, and Wallace[19] (MRW) in Fig. 17. Although EI-1 pushes the ^{12}C cross section to large angles too strongly, the analyzing-power and spin-rotation predictions are better than those of the MRW model.

It is clear from the above comparison that elastic scattering alone cannot distinguish between Dirac and Schrödinger descriptions of proton scattering. Both approaches yield similar results for the density dependence of the effective interaction. Although we have not established a formal relationship between the Schrödinger-equivalent potentials and the present effective interaction, the close similarity between these results suggests that it may be profitable to derive such a relationship. Addi-

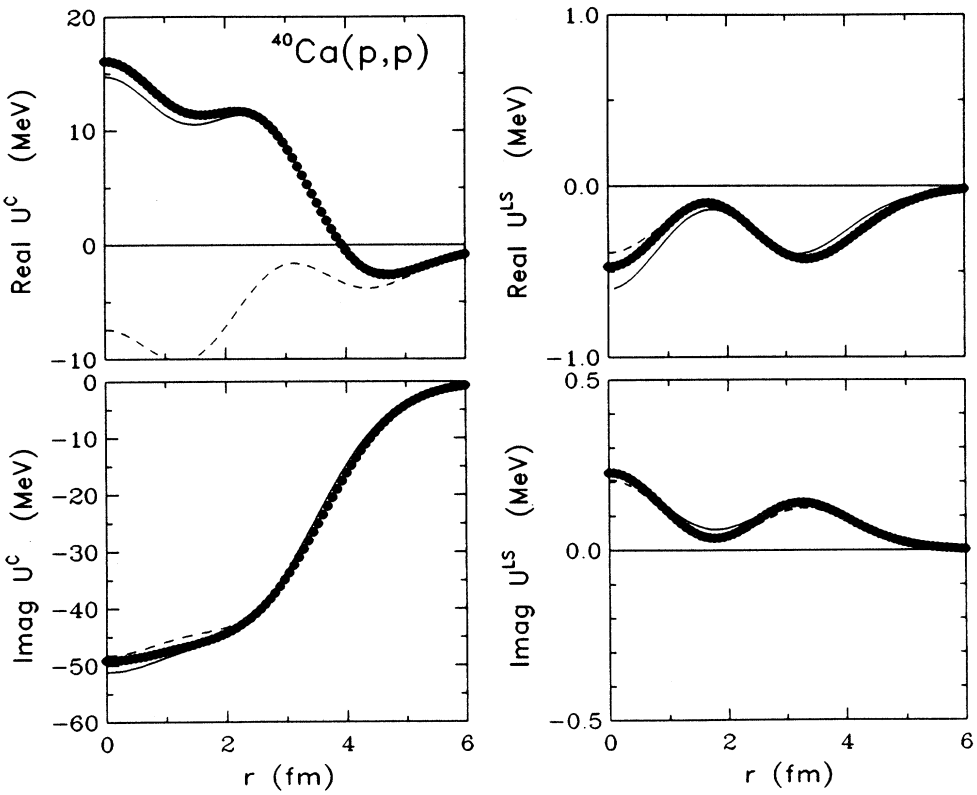

FIG. 15. Components of the optical potential for 500-MeV protons on ^{40}Ca. The dashed lines and circles are, respectively, the equivalent Schrödinger potentials for the (NRIA) no-pair interaction and the relativistic 1A2 interaction of Ref. 5, whereas the solid lines employ empirical interaction EI-1.

tional medium modifications beyond the pair contribution could then be added as (presumably) small corrections. Cheon and Takayanagi[43] have developed a simple schematic model in which both medium and relativistic corrections to the central component of the t matrix are added in the form

$$t^{\rm el}(q,\rho)=t(q,0)+\delta t^{\rm el}_{\rm MC}(q,\rho)+\delta t^{\rm el}_{\rm RC}(q,\rho)\ , \tag{16a}$$

$$t^{\rm in}(q,\rho)=\left[1+\rho\frac{\partial}{\partial\rho}\right]t^{\rm el}(q,\rho)\ , \tag{16b}$$

where "el" stands for elastic, "in" for inelastic, "MC" for medium correction, and "RC" for relativistic correction. Note that the rearrangement factor applies to both medium and relativistic corrections. The medium correction incorporates Pauli blocking based upon the nonrelativistic G matrix. The relativistic correction was derived by comparing Dirac and Schrödinger-equivalent folding-model potentials for infinite nuclear matter and has the form

$$\delta t^{\rm el}_{\rm RC}(\rho)=\frac{\mathcal{S}^2-\mathcal{V}^2}{2E}\rho\ , \tag{17}$$

where $\mathcal{S}$ and $\mathcal{V}$ are the strengths of the Dirac scalar and vector interactions at $q=0$. According to Cheon and Takayanagi,[43] the MRW[19] amplitudes give

$$\rho_0\mathcal{S}=(-295+75i)\ \text{MeV fm}^3\ , \tag{18a}$$

$$\rho_0\mathcal{V}=(185-90i)\ \text{MeV fm}^3\ , \tag{18b}$$

so that

$$\delta t^{\rm el}_{\rm RC}(\rho)=(113-22i)\rho/\rho_0\ \text{MeV fm}^3\ , \tag{19}$$

at 500 MeV. This correction is essentially a dispersion effect due to the effective mass in the medium. The real part is stronger than the nonrelativistic result of Ray, but is in good agreement with the present phenomenology. The imaginary part has the same sign as the corresponding phenomenological parameter, but is significantly smaller. Moreover, we also should include a Pauli blocking correction of the opposite sign.

B. Comparison with Dirac phenomenology

Global optical potentials for use in the Dirac equation have been fitted to proton elastic-scattering data for heavy targets in the energy regime $65\le E_p\le 1040$ MeV. The scalar and vector potentials are represented by simple radial functions with geometries similar to the conventional Woods-Saxon potential, and the strengths and geometric parameters are expressed as functions of both mass and energy. Excellent fits were obtained to cross-

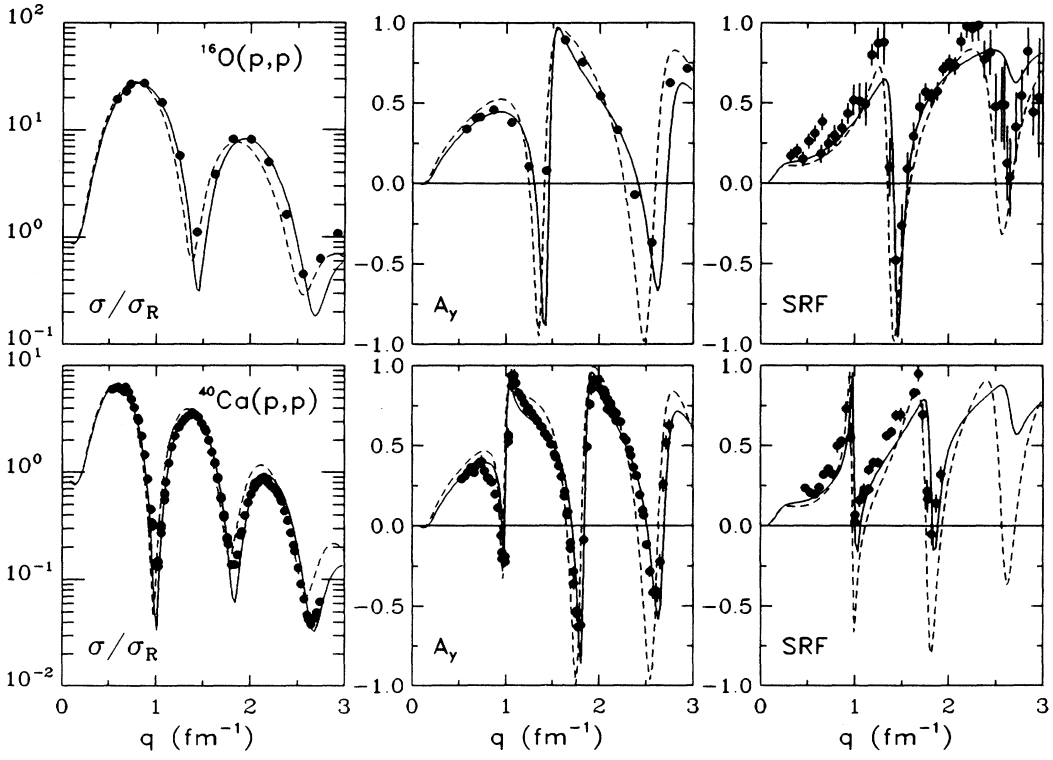

FIG. 16. Differential cross-section (presented as the ratio to Rutherford to enhance detail), analyzing-power, and spin-rotation function data for proton elastic scattering from ^{16}O and ^{40}Ca are compared with the predictions of the IA2 analysis of Ref. 5 (dashed lines) and predictions with the empirical interaction EI-1 (solid lines).

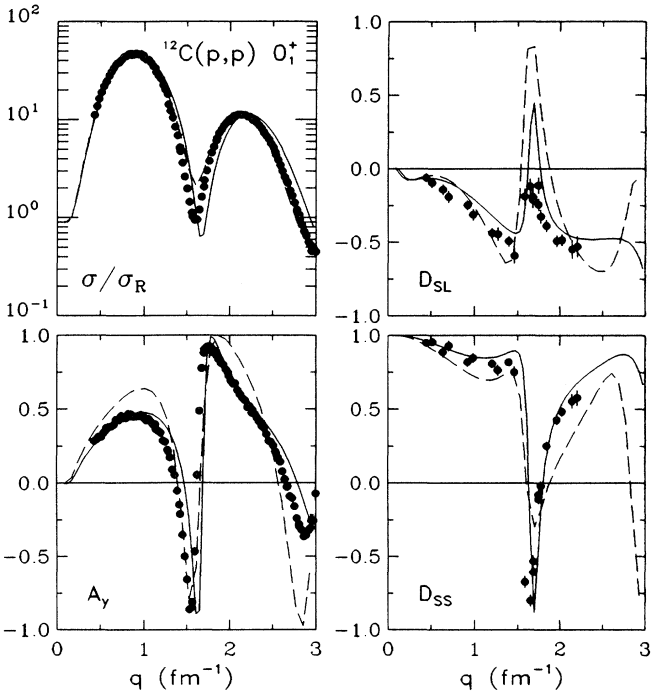

FIG. 17. Calculations based upon empirical interaction EI-1 (solid) and MRW relativistic impulse approximation (dashed) are compared with data from Ref. 50 for the elastic scattering of 494-MeV protons by ^{12}C.

section, analyzing-power, and spin-rotation data for ^{40}Ca and ^{208}Pb, including data that were omitted from the analysis. It is of interest to compare the Schrödinger potentials equivalent to the Dirac phenomenological optical potential (DPOP) fitted to data for elastic scattering with the potentials produced by our analysis of inelastic-scattering data.

The Schrödinger potentials equivalent to the "fit-1" version of the Dirac phenomenology for ^{40}Ca at 500 MeV are compared in Fig. 18 with potentials calculated from the interactions presented in Sec. IV. The spin-orbit potentials and imaginary part of the central potential are determined uniquely by fits to the inelastic-scattering data and agree with the global Dirac potentials for $r \gtrsim 3$ fm. For $r \lesssim 3$ fm, the ImU^C produced by the empirical effective interaction is about 25% stronger than predicted by Dirac phenomenology.

The real part of the central potential appears to be poorly determined by inelastic-scattering data. It is interesting to observe that the fits that include data for ^{16}O, either alone or in conjunction with ^{40}Ca data, agree better with the ^{40}Ca DPOP potential than does the fit made to ^{40}Ca data alone. As previously suggested, stronger absorption by heavier nuclei limits interior sensitivity and can apparently lead to unnecessarily strong repulsion in Ret^C.

We based most of the preceding discussions upon interaction EI-1 for several reasons. First, our experience has shown that fits to ^{16}O data generally produce more stable and reliable results than fits to data for heavier nuclei. Second, the repulsive component is less severe in EI-1 than in the other interactions and is more consistent with the trend displayed by fits made for lower energies. Third, EI-1 compares most favorably with the IA2 model, a microscopic theory with a sound foundation. Interaction EI-1A fitted to ^{16}O data subject to the constraint $S_1 \approx 0.88$ gives a similar result for b_1 and similar fits to the data, but produces a stronger ReU^C in the interior that is about midway between the DPOP and IA2 potentials. The other empirical interactions and DPOP potential all suggest even stronger repulsion than either EI-1 or IA2.

It is well known from numerous nonrelativistic analyses that optical potentials fitted to elastic-scattering data are prone to both discrete and continuous ambiguities. Because elastic observables depend only upon the asymptotic wave function, any potential which produces the same phase shifts will produce the same elastic scattering. Hence elastic scattering is not directly sensitive to the shape of the potential or the nature of the wave function in the interior. Inelastic scattering, by contrast, depends upon the overlap between distorted waves and a transition density and, hence, is directly sensitive to the interior wave function. Therefore, our method of fitting an effective interaction to inelastic-scattering data is more sensitive to the interior potential than is elastic scattering itself, especially when accurate data for states with interior transition densities are available.

Although the potential fitted to elastic-scattering data produces a better χ^2 fit to that data than our potentials, this fact does not guarantee that those potentials provide a better representation of the physics described by the first-order optical potential. Furthermore, there is no guarantee that there does not exist an alternative set of potentials in a χ^2 minimum that is nearly as deep, but which resembles the results of our model more closely. It is not implausible to suggest that had the fit begun with a deeper imaginary potential or had that potential been constrained to the neighborhood of our model, then perhaps a shallower real potential closer to the IA2 model might have emerged as a fit nearly as good as that chosen by Hama *et al.*[21] This type of compensation is characteristic of phenomenological optical potentials.

C. Comparison with the relativistic RPA

Few relativistic calculations beyond the collective model have been performed for inelastic scattering, in part because of the difficulties in relativistic models for nuclear structure. An exception is the Dirac random-phase-approximation (RPA) calculation performed by Rost and Shepard for the 3_1^- and 5_1^- states of ^{40}Ca.[59] Their results for the depolarization data are nearly as good as the calculations shown here in Figs. 8 and 9. However, this model gives a cross section well below the data at the peak of the 5^- angular distribution, revealing deficiencies in the RPA model of the structure. Fortunately, the D_{ij} calculations for collective excitations are relatively insensitive to details of nuclear structure when only the matter density contributes. Hence these quanti-

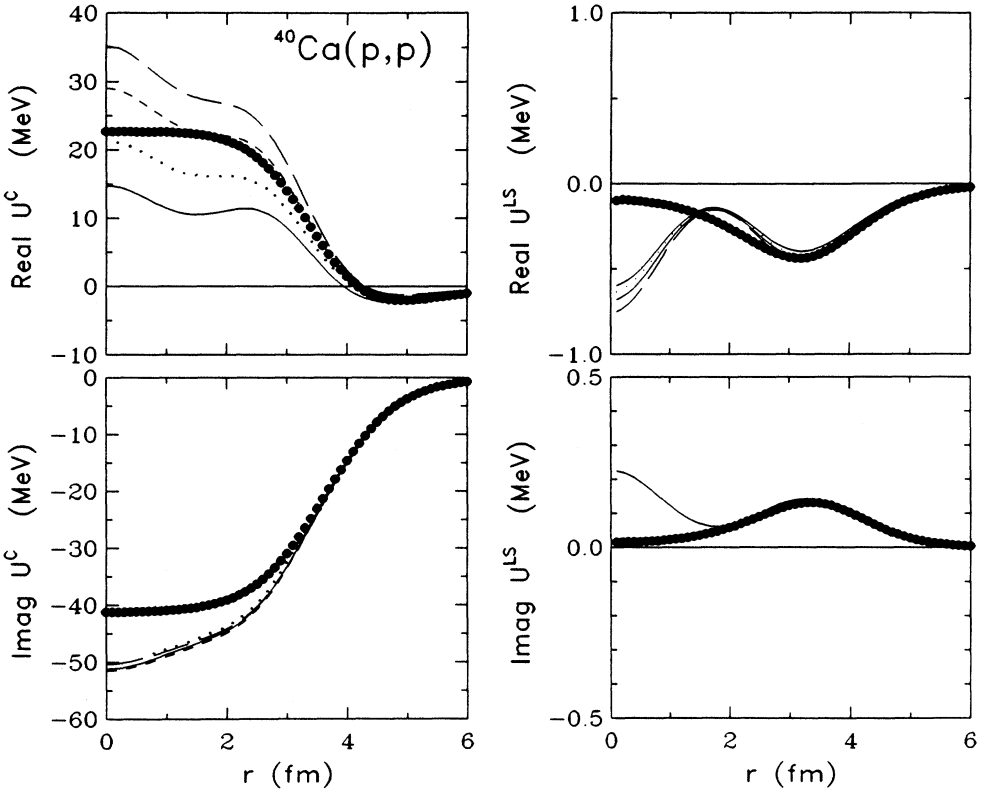

FIG. 18. Schrödinger-equivalent potentials from Dirac phenomenology are compared with optical potentials for ^{40}Ca at 500 MeV calculated from several versions of the empirical effective interaction. The solid circles display Dirac potentials from "fit 1" of Ref. 21. The curves correspond to effective interaction EI-1 (solid), EI-1A (dots), EI-2 (long dashes), and EI-3 (short dashes). Note that the solid curves correspond most closely to the IA2 potentials shown in Fig. 15.

ties are primarily sensitive to properties of the effective interaction that are quite similar for the RIA and for our empirical effective interaction. Our cross-section calculations are more accurate because we use experimental rather than theoretical transition densities.

D. Self-consistency

Amado *et al.*[60] have shown that cross sections and analyzing powers for collective transitions can, under appropriate conditions, be derived from elastic scattering with good accuracy. The validity of these data-to-data relationships requires energies above 500 MeV and nuclei large enough for transition densities to be related by the Tassie model to a Fermi distribution. However, these relationships fail to describe scattering by more general transition densities, such as the 3_2^- transition of ^{40}Ca, or by light nuclei, such as ^{16}O.

The success of the present analysis can be interpreted as a demonstration of a more general data-to-data relationship based on a realistic reaction model rather than on an unrealistic structure model. The rearrangement factor $(1+\rho\,\partial/\partial\rho)$ relates the effective interaction for inelastic scattering to the corresponding interaction for elastic scattering self-consistently. Based upon this relationship, we are able to predict elastic scattering by analyzing inelastic scattering. Not only can we tolerate interior transition densities for light nuclei, but the analysis is enhanced considerably by their inclusion. Therefore, we conclude that the rearrangement factor proposed by Cheon, Takayanagi, and Yazaki[42,43] represents a more powerful data-to-data relationship than the model of Amado *et al.*[60]

VI. CONCLUSIONS

The radial sensitivity of inelastic scattering provides a powerful probe of medium modifications to the nucleon-nucleon effective interaction. Using electroexcitation to determine nuclear transition densities allows one to investigate this effective interaction with little residual uncertainty due to nuclear structure. Inelastic proton scattering which excites states with transition densities peaked both at the surface and in the interior probes both the low- and high-density properties of the effective interaction. Additional radial sensitivity is obtained by evaluating self-consistently the optical potential for elastic scattering. An analysis of inelastic-scattering data that employs several states of each character can determine the density dependence of the effective interaction with little ambiguity.

In earlier work we developed a simple parametrization of medium modifications to the effective interaction capable of representing any of the G-matrix calculations then

available for energies below 400 MeV. In this paper we show that the same function also describes a recent theoretical effective interaction calculated by Ray that, by including inelasticity, is applicable to energies above pion threshold. However, for predictions of inelastic proton scattering, this theoretical interaction provides only modest improvement over the nonrelativistic impulse approximation, which underestimates cross sections for states with interior transition densities at all momentum transfers and for states with surface densities at high q. Analyzing powers computed from this theoretical interaction are too strong for low q and generally exhibit oscillations that are too severe. Therefore, we fitted the parameters of an empirical effective interaction to scattering data for 500-MeV protons.

The result of our fit to the data is an empirical interaction that describes many transitions in ^{16}O simultaneously; this same interaction describes elastic scattering also. To describe the inelastic-scattering data, an interaction with a strong dependence on the local density in the interaction region is required. This result is independent of the form of parametrization used for the empirical interaction. The dependence on density is much stronger than that of the theoretical interaction of Ray; the strength of the real part of the central component of the interaction is stronger than that predicted by the theoretical interaction, and the strength of the imaginary part is contrary to the Pauli blocking effect in the Ray interaction. This enhancement of the absorption in the empirical interaction was observed in a similar analysis at 318 MeV also, indicating a new absorptive mechanism not present in existing theoretical models.

Optical potentials computed from the empirical interaction are almost identical with the Schrödinger-equivalent potentials computed from the relativistic IA2 model of Ottenstein, Wallace, and Tjon,[5] but are not in agreement with either the free interaction or the Ray interaction. Thus the general features of the empirically determined density dependence are in agreement with the virtual pair contribution of the IA2 model. This is observed most noticeably in the large repulsive contribution to the real central interaction. The similarity between these models of the optical potential suggests that it should be possible, and more economical, to reparametrize the IA2 model in terms of an effective interaction of the present type.

Another feature of the empirical interaction which is consistent with similar empirical analyses at lower energies is that the scale factors for each of the terms are not equal to one. Thus the empirical interaction does not heal to the free interaction at zero density, a finding which is not consistent with a strict interpretation of the LDA. We have speculated[15,16] that this effect may reflect a nonlocality correction to the LDA due to effects of the radial extent of nuclear orbitals in finite nuclei. In particular, it is reasonable to expect the effective interaction for finite nuclei to exhibit stronger density dependence for low densities and weaker density dependence at high densities than predicted for infinite nuclear matter with the corresponding density.

The interaction fitted to inelastic scattering from ^{16}O was found to predict both elastic and inelastic scattering from ^{40}Ca with remarkable accuracy, including the features in the analyzing-power and spin-rotation data that heretofore could be understood using relativistic calculations only. We find also that interactions fitted to data for ^{40}Ca or for the combined ^{40}Ca and ^{16}O data set produce predictions for scattering observables that are very similar to those predicted by the interaction fitted to the data for ^{16}O alone. Also, the interaction fitted to the inelastic ^{16}O transitions predicts elastic-scattering observables for ^{12}C and ^{208}Pb with remarkable accuracy. Therefore, these results support the LDA hypothesis that the effective interaction depends upon local density, but not upon the specific transition or target. Furthermore, the accuracy of elastic-scattering predictions based on an interaction fitted to inelastic-scattering data supports the validity of the Cheon self-consistency relationship. In effect, the rearrangement factor constitutes a powerful data-to-data relationship.

Further insight into the proper interpretation of these phenomenological results awaits development of a detailed theoretical model capable of including Pauli blocking, self-energy corrections, *NN* inelasticity, and relativistic dynamics in a self-consistent model of the effective interaction for finite nuclei. The success of the empirical effective interaction in describing both elastic and inelastic scattering for the energy range 100–500 MeV with the same density dependence for all nuclei suggests that a simple parametrization should be possible and may explain the values extracted from the data. In the meantime the empirical effective interaction provides a useful tool for extracting accurate neutron transition densities from proton-scattering data.[61]

ACKNOWLEDGMENTS

We thank Dr. K. K. Seth and Dr. J. Lissanti for tables of inelastic-scattering data for $p+^{40}$Ca at 500 MeV. We thank Dr. N. Ottenstein and Dr. S. J. Wallace for tables of their IA2 optical potentials, and Dr. L. Ray for tables of his effective interaction. Finally, we thank Dr. S. Hama for a subroutine codifying the Dirac global optical potential. This work was supported by grants from the National Science Foundation and the Department of Energy.

[a]Present address: Argonne National Laboratory, Argonne, IL 60439.

[b]Present address: Rogaland Research Institute, Stavanger, Norway.

[c]Present address: Allied-Signal, Los Angeles, CA 90504.

[d]Present address: California State University, Hayward, CA 94542.

[e]Present address: University of South Carolina, Columbia, SC

29208.
[f]Present address: College of William & Mary, Williamsburg, VA 23185.
[g]Present address: University of Washington, Seattle, WA 98195.
[h]Present address: University of Virginia, Charlottesville, VA 22901.
[i]Present address: CEBAF, Newport News, VA 23606.
[1]A. K. Kerman, H. McManus, and R. M. Thaler, Ann. Phys. (N.Y.) **8**, 551 (1959).
[2]M. A. Franey and W. G. Love, Phys. Rev. C **31**, 488 (1985).
[3]For example, W. G. Love, in *Workshop on Relations Between Reactions and Structure in Nuclear Physics,* edited by D. H. Feng, M. Vallieres, and B. H. Wildenthal (World Scientific, Singapore, 1987), p. 293; J. J. Kelly, in *ibid.*, p. 222; F. Petrovich, J. A. Carr, and H. McManus, Annu. Rev. Nucl. Part. Sci. **36**, 29 (1986).
[4]L. Ray, Phys. Rev. C **41**, 2816 (1990).
[5]N. Ottenstein, S. J. Wallace, and J. A. Tjon, Phys. Rev. C **38**, 2272 (1988); **38**, 2289 (1988).
[6]J. Kelly, W. Bertozzi, T. N. Buti, F. W. Hersman, C. Hyde, M. V. Hynes, B. Norum, F. N. Rad, A. D. Bacher, G. T. Emery, C. C. Foster, W. P. Jones, D. W. Miller, B. L. Berman, W. G. Love, and F. Petrovich, Phys. Rev. Lett. **45**, 2012 (1980).
[7]F. A. Brieva and J. R. Rook, Nucl. Phys. **A291**, 299, 317 (1977); **A297**, 206 (1978); **A307**, 493 (1978); H. V. von Geramb, F. A. Brieva, and J. R. Rook, in *Microscopic Optical Potentials,* edited by H. V. von Geramb (Springer-Verlag, Berlin, 1979), p. 104.
[8]H. V. von Geramb, in *The Interaction Between Medium Energy Nucleons in Nuclei (Indiana Cyclotron Facility, Bloomington, Indiana),* Proceedings of the Workshop on the Interactions Between Medium Energy Nucleons in Nuclei, AIP Conf. Proc. No. 97, edited by H. O. Meyer (AIP, New York, 1983), p. 44; L. Rikus, K. Nakano, and H. V. von Geramb, Nucl. Phys. **A414**, 413 (1984).
[9]K. Nakayama and W. G. Love, Phys. Rev. C **38**, 51 (1988).
[10]J. Hüfner and C. Mahaux, Ann. Phys. (N.Y.) **73**, 525 (1972).
[11]J. J. Kelly, W. Bertozzi, T. N. Buti, J. M. Finn, F. W. Hersman, C. E. Hyde-Wright, M. V. Hynes, M. A. Kovash, B. Murdock, B. E. Norum, B. Pugh, F. N. Rad, A. D. Bacher, G. T. Emery, C. C. Foster, W. P. Jones, D. W. Miller, B. L. Berman, W. G. Love, J. A. Carr, and F. Petrovich, Phys. Rev. C **39**, 1222 (1989).
[12]K. M. Watson, Phys. Rev. **89**, 575 (1953).
[13]E. L. Lomon and H. Feshbach, Ann. Phys. (N.Y.) **48**, 94 (1968); E. L. Lomon, Phys. Rev. D **26**, 576 (1982).
[14]J. J. Kelly, Phys. Rev. C **37**, 520 (1988); J. A. Carr, F. Petrovich, and J. Kelly, in *Neutron-Nucleus Collisions—A Probe of Nuclear Structure (Burr Oak State Park, Glouster, Ohio),* Proceedings of the Conference on Neutron-Nucleus Collisions—A Probe of Nuclear Structure, AIP Conf. Proc. No. 124, edited by J. Rapaport, R. W. Finlay, S. M. Grimes, and F. Dietrich (AIP, New York, 1985), p. 230.
[15]J. J. Kelly, Phys. Rev. C **39**, 2120 (1989).
[16]J. J. Kelly, J. M. Finn, W. Bertozzi, T. N. Buti, F. W. Hersman, C. Hyde-Wright, M. V. Hynes, M. A. Kovash, B. Murdock, P. Ulmer, A. D. Bacher, G. T. Emery, C. C. Foster, W. P. Jones, D. W. Miller, and B. L. Berman, Phys. Rev. C **41**, 2504 (1990); Q. Chen, J. J. Kelly, P. P. Singh, M. C. Radhakrishna, W. P. Jones, and H. Nann, *ibid.* **41**, 2514 (1990).
[17]J. J. Kelly, A. E. Feldman, B. S. Flanders, H. Seifert, D. Lopiano, B. Aas, A. Azizi, G. Igo, G. Weston, C. Whitten, A. Wong, M. V. Hynes, J. McClelland, W. Bertozzi, J. M. Finn, C. E. Hyde-Wright, R. W. Lourie, P. E. Ulmer, B. E. Norum, and B. L. Berman, Phys. Rev. C **43**, 1272 (1991).
[18]H. Seifert, Ph.D. thesis, University of Maryland, 1990.
[19]J. A. McNeil, L. Ray, and S. J. Wallace, Phys. Rev. C **27**, 2123 (1983).
[20]L. G. Arnold, B. C. Clark, R. L. Mercer, and P. Schwandt, Phys. Rev. C **23**, 1949 (1981); L. G. Arnold, B. C. Clark, and R. L. Mercer, *ibid.* **23**, 15 (1981); B. C. Clark, R. L. Mercer, and P. Schwandt, Phys. Lett. **122B**, 211 (1983); B. C. Clark, S. Hama, and R. L. Mercer, in *The Interaction Between Medium Energy Nucleons in Nuclei* (Ref. 8), p. 260.
[21]S. Hama, B. C. Clark, E. D. Cooper, H. S. Sherif, and R. L. Mercer, Phys. Rev. C **41**, 2737 (1990).
[22]D. P. Murdock and C. J. Horowitz, Phys. Rev. C **35**, 1442 (1987).
[23]M. V. Hynes, A. Picklesimer, P. C. Tandy, and R. M. Thaler, Phys. Rev. Lett. **52**, 978 (1984); M. V. Hynes, A. Picklesimer, P. C. Tandy, and R. M. Thaler, Phys. Rev. C **31**, 1438 (1985).
[24]E. E. van Faassen and J. A. Tjon, Phys. Rev. C **28**, 2354 (1983); **30**, 285 (1984).
[25]L. G. Atencio, J. F. Amann, R. L. Boudrie, and C. L. Morris, Nucl. Instrum. Methods **187**, 381 (1981).
[26]J. B. McClelland, J. F. Amann, W. D. Cornelius, and H. A. Thiessen, Los Alamos Scientific Laboratory Report No. LA-UR 84-1671, 1984.
[27]R. A. Arndt, program SAID (unpublished); R. A. Arndt, L. D. Roper, R. A. Bryan, R. B. Clark, B. J. VerWest, and P. Signell, Phys. Rev. D **28**, 97 (1983).
[28]M. W. McNaughton, Los Alamos Scientific Laboratory Report No. LA-8307, 1980.
[29]J. J. Kelly, computer program ALLFIT (unpublished).
[30]S. Dixit, W. Bertozzi, C. Hyde-Wright, J. Kelly, M. V. Hynes, B. E. Norum, J. M. Finn, M. A. Kovash, F. W. Hersman, A. D. Bacher, G. T. Emery, C. C. Foster, W. P. Jones, D. W. Miller, and B. L. Berman, Phys. Rev. C **43**, 1758 (1991).
[31]F. Ajzenberg-Selove, Nucl. Phys. **A375**, 1 (1982).
[32]D. Lopiano, Ph.D. thesis (UCLA draft).
[33]D. Besset, B. Favier, L. G. Greeniaus, R. Hess, C. Lechanoine, D. Rapin, and D. W. Werren, Nucl. Instrum. Methods **166**, 515 (1979).
[34]B. Aas, E. Bleszynski, M. Bleszynski, M. Hajisaeid, G. J. Igo, F. Irom, G. Pauletta, A. Rahbar, A. T. M. Wang, J. F. Amann, T. A. Carey, W. D. Cornelius, J. B. McClelland, M. Barlett, G. W. Hoffmann, and M. Gazzaly, Nucl. Phys. **A460**, 675 (1986).
[35]See AIP document No. PAPS PRVCA-43-2103-8 for eight pages containing a complete tabulation of the data described in this paper. Order by PAPS number and journal reference from American Institute of Physics, Physics Auxiliary Publication Service, 335 E. 45th Street, New York, NY 10017. The price is $1.50 for each microfiche or $5.00 for photocopies. Air mail additional. Make checks payable to the American Institute of Physics.
[36]J. J. Kelly, in *Advanced Methods in the Evaluation of Nuclear Scattering Data,* Vol. 236 of *Lecture Notes in Physics,* edited by H. J. Krappe and R. Lipperheide (Springer-Verlag, Berlin, 1985), p. 335; J. J. Kelly, in *Current Problems in Nuclear Physics,* edited by T. Paradellis and S. Kossionides (Hellenic Physical Society Conference, Athens, 1986), Vol. 1, p. 325; J. J. Kelly, in *Nuclear Structure At High Spin, Excitation, and Momentum Transfer (McCormick's Creek State Park, Bloomington, Indiana),* Proceedings of the Workshop on Nuclear Structure at High Spin, Excitation and Momentum Transfer, AIP Conf. Proc. No. 142, edited by H. Nann (AIP, New

York, 1986), p. 27.
[37]F. Petrovich, R. J. Philpott, A. W. Carpenter, and J. A. Carr, Nucl. Phys. **A425**, 609 (1984).
[38]T. N. Buti, J. Kelly, W. Bertozzi, J. M. Finn, F. W. Hersman, C. Hyde-Wright, M. V. Hynes, M. A. Kovash, S. Kowalski, R. W. Lourie, B. Murdock, B. E. Norum, B. Pugh, C. P. Sargent, W. Turchinetz, and B. L. Berman, Phys. Rev. C **33**, 755 (1986).
[39]R. A. Miskimen, Ph.D. thesis, Massachusetts Institute of Technology, 1983.
[40]C. Williamson *et al.* (unpublished).
[41]H. deVries, C. W. deJager, and C. deVries, At. Data Nucl. Data Tables **36**, 495 (1987).
[42]T. Cheon, K. Takayanagi, and K. Yazaki, Nucl. Phys. **A437**, 301 (1985); **A445**, 227 (1985).
[43]T. Cheon and K. Takayanagi, Nucl. Phys. **A455**, 653 (1986).
[44]E. Clementel and C. Villi, Nuovo Cimento **2**, 176 (1955).
[45]K. K. Seth, D. Barlow, A. Saha, R. Soundranayagam, S. Iversen, M. Kaletka, M. Basko, D. Smith, G. W. Hoffman, M. L. Barlett, R. Fergerson, J. McGill, and E. C. Milner, Phys. Lett. **158B**, 23 (1985).
[46]J. Lisantti, D. J. Horen, F. E. Bertrand, R. L. Auble, B. L. Burks, E. E. Gross, R. O. Sayer, D. K. McDaniels, K. W. Jones, J. B. McClelland, S. J. Seestrom-Morris, and L. W. Swenson, Phys. Rev. C **39**, 568 (1989).
[47]F. Petrovich, J. A. Carr, R. J. Philpott, A. W. Carpenter, and J. Kelly, Phys. Lett. **165B**, 19 (1985).
[48]J. A. McNeil, J. R. Shepard, and S. J. Wallace, Phys. Rev. Lett. **50**, 1439 (1983); J. R. Shepard, J. A. McNeil, and S. J. Wallace, *ibid.* **50**, 1443 (1983).
[49]B. C. Clark, S. Hanna, R. L. Mercer, L. Ray, and B. D. Serot, Phys. Rev. Lett. **50**, 1644 (1983).
[50]G. W. Hoffman, M. L. Barlett, D. Ciskowski, G. Pauletta, M. Purcell, L. Ray, J. F. Amann, J. Jarmer, K. W. Jones, S. Penttilä, N. Tanaka, M. M. Gazzaly, J. R. Comfort, B. C. Clark, and S. Hama, Phys. Rev. C **41**, 1651 (1990).
[51]G. W. Hoffman, L. Ray, M. L. Barlett, R. Fergerson, J. McGill, E. C. Milner, K. K. Seth, D. Barlow, M. Bosko, S. Iverson, M. Kaletka, A. Saha, and D. Smith, Phys. Rev. Lett. **47**, 1436 (1981).
[52]L. Ray and G. W. Hoffman, Phys. Rev. C **31**, 538 (1985).
[53]J. Dechargé and D. Gogny, Phys. Rev. C **21**, 1568 (1980); J. Dechargé, M. Girod, D. Gogny, and B. Grammaticos, Nucl. Phys. **A358**, 203c (1981).
[54]H. F. Arellano, F. A. Brieva, and W. G. Love, Phys. Rev. Lett. **63**, 605 (1989); Phys. Rev. C **41**, 2188 (1990).
[55]Ch. Elster and P. C. Tandy, Phys. Rev. C **40**, 881 (1989); Ch. Elster, T. Cheon, E. F. Redish, and P. C. Tandy, *ibid.* **41**, 814 (1990).
[56]N. Ottenstein, E. E. van Faassen, J. A. Tjon, and S. J. Wallace, Phys. Rev. C **43**, 2393 (1991).
[57]M. L. Barlett, W. R. Coker, G. W. Hoffman, and L. Ray, Phys. Rev. C **29**, 1407 (1984); M. L. Barlett, G. W. Hoffman, and L. Ray, *ibid.* **35**, 2185 (1987).
[58]C. J. Horowitz and B. D. Serot, Nucl. Phys. **A368**, 503 (1981).
[59]E. Rost and J. R. Shepard, Phys. Rev. C **40**, 1736 (1989).
[60]R. D. Amado, F. Lenz, J. A. McNeil, and D. A. Sparrow, Phys. Rev. C **22**, 2094 (1980); R. D. Amado, J. A. McNeil, and D. A. Sparrow, *ibid.* **23**, 2114 (1981); J. A. McNeil and D. A. Sparrow, *ibid.* **23**, 2124 (1981).
[61]J. J. Kelly, Q. Chen, P. P. Singh, M. C. Radhakrishna, W. P. Jones, and H. Nann, Phys. Rev. C **41**, 2525 (1990).